

A low glyceamic diet protects disease-prone Nrf2-deficient mice against age-related macular degeneration

Sheldon Rowan, Shuhong Jiang, Min-Lee Chang, Jonathan Volkin, Kelsey M. Smith, Carlos Moreira-Neto, Naila Rabanni, Paul J. Thornalley, Donald E. Smith, Nadia K. Waheed, Allen Taylor

Abstract

Age-related macular degeneration (AMD) is a major blinding disease, affecting over 14% of the elderly. Risk for AMD is related to age, diet, environment, and genetics. Dietary modulation of AMD risk is a promising treatment modality, but requires appropriate animal models to demonstrate advantages of diet. Mice lacking the antioxidant transcription factor Nrf2 develop age-related retinopathy resembling human AMD. Here we evaluated the effect of consuming high glyceamic (HG) or low glyceamic (LG) diets until 18-months of age on development of AMD in Nrf2-null mice. Nrf2-null mice that consumed HG diets developed atrophic AMD, characterized by photoreceptor degeneration, retinal pigment epithelium (RPE) atrophy and pigmentary abnormalities, basal deposits, and degeneration of the choroidal vasculature. In contrast, Nrf2-null-mice that consumed LG diets did not develop overt retinal disease phenotypes. Consumption of HG diets was associated with accumulation of advanced glycation end-products systemically including within the RPE, whereas consumption of the LG diet was associated with increased levels of anti-glycative and anti-oxidative detoxification machinery. Together our data indicate that the Nrf2-null HG mouse is a good model for atrophic AMD studies and that the LG diet can activate protective pathways to prevent AMD, even in a genetically predisposed animal.

Introduction

Age-related macular degeneration (AMD) is the leading cause of blindness in industrialized nations and prevalence of AMD is accelerating due to increasingly aging populations globally and a changing food environment. Advanced AMD can be neovascular (wet AMD), comprising approximately 15% of cases, or atrophic (dry AMD), accounting for approximately 85% of cases. Whereas neovascular AMD can be treated using anti-angiogenic agents, there is no current treatment for advanced atrophic AMD, in which the retinal pigmented epithelium (RPE) degenerates, leading to loss of photoreceptor cells and subsequent visual dysfunction. Often, diagnosis only follows some loss of vision, making prevention challenging. A dearth of biomarkers for early AMD compounds this frustration.

Progression of intermediate to advanced AMD can be slowed via the AREDS2 supplements containing high doses of vitamin A, vitamin E, zinc, lutein, and zeaxanthin (1). Epidemiological evidence supports the notion that a healthy diet can prevent early AMD and progression to advanced AMD (2-4). In particular, consumption of healthy dietary patterns like the Mediterranean diet or low glyceamic index diets seem to protect against AMD (5-9) (4, 10), whereas consumption of a Western dietary pattern or high glyceamic index diets appear to increase risk for AMD (6, 11-13). Many of these findings have been corroborated experimentally in disease model systems, notably in mouse and primate models (14-17).

Understanding more about the etiology of AMD would inform about ways to delay onset or progress of the disease. Pathomechanistic investigations of AMD have been enhanced by

utilization of genetic and cellular model disease systems. Studies in mice and human RPE cells have shown that oxidative damage, lipid accumulation, mitochondrial dysfunction, inflammatory damage, and loss of protein quality control all contribute to AMD pathogenesis (18-23). Many of these mechanisms are recapitulated by dietary stress. Wildtype mice fed a high glycemic (HG) diet and aged to 24-months develop features of AMD, which can be arrested, and possibly even reversed, by dietary change to a low glycemic (LG) diet (17). We proposed that among mechanisms behind the HG diet-AMD connection is glycation-induced modification of bulk proteins, including accumulation of advanced glycation end-products (AGEs) in the eye (16, 17, 24). AGEs are formed by non-enzymatic reaction of sugars or their catabolites with proteins and other biomolecules compounded by oxidative and other stresses. Collectively these modifications are called glycation. AGEs are cytotoxic and have been shown to be increased locally and systemically in AMD (25-29). Accumulation of AGEs compounds cellular vulnerability by protein quality control processes that remove aggregated and damaged protein and lipid species (24, 30). Formation of AGEs can be limited by either reducing glycemia or by reducing oxidative stress; both mechanisms also appear to reduce risk for AMD (1, 31).

Nrf2 is a transcription factor that controls critical antioxidant responses to environmental and cellular stresses. As antioxidant responses, Nrf2 target genes increase major antioxidant systems including glutathione and thioredoxin, phase I and phase II detoxification machinery, NADPH regeneration, heme and iron metabolism (32). Nrf2 also activates glyoxalase I, which detoxifies precursors of AGEs, including methylglyoxal, the major glycating product of glucose catabolism, thus preventing AGE formation (33-36). Nrf2 itself is glycated, leading to diminution of its antioxidant function (37). Nrf2 also participates in regulation of metabolic and autophagic pathways, which together preserve protein quality control and cellular health (38, 39). Some of these activities are attributable to functions of Nrf2 in maintenance of mitochondrial biogenesis, distribution, and function (39-41). Nrf2 regulates mitochondrial biogenesis in concert with PGC-1 α , a critical transcriptional regulator of mitochondrial biogenesis (42). Consistent with these diverse cellular functions, loss of Nrf2 in mice damages many organs systems like the liver, lung, and brain, and predisposes mice to several neoplasias (43-47).

In the eye, loss of Nrf2 renders mice susceptible to vascular damage caused by ischemia-reperfusion injury (48). Aged Nrf2-deficient eyes undergo retinopathy between 12-15 mo., including AMD features (49). AMD-like phenotypes are worsened by combined loss of Nrf2 and PGC1 α . Together these suggest that mitochondrial damage and reactive oxygen species generation caused by PGC1 α deficiency, coupled with an impaired antioxidant response caused by Nrf2 deficiency lead to AMD pathogenesis (50). Conversely, overexpression of Nrf2 can rescue retinal degeneration in an inherited model of retinitis pigmentosa (51). Nrf2 can also be activated by other cytoprotective pathways, like the sigma1 receptor chaperone, to rescue cone photoreceptor degeneration (52). In response to dietary and environmental stresses and aging, Nrf2 function declines, contributing to RPE degenerative processes, like those occurring in geographic atrophy, a late form of dry AMD (53, 54).

Here we sought to understand the interaction of diet-induced glycemia, as elicited by the same amount of dietary carbohydrate, but that is less or more readily digested, on age-related retinal health within the context of Nrf2 deficiency. Specifically, we tested the hypothesis that feeding Nrf2-null mice a HG, but not LG, diet would induce glycemic and glycative stresses that would lead to progressive eye pathology. We also tested whether the LG diet could exhibit salutary functions in an Nrf2-independent fashion. We found that Nrf2-null mice fed HG diets developed atrophic AMD-like disease but Nrf2-null mice fed LG diets

were protected from retinopathy at 18-months of age. Therefore, Nrf2-null mice fed HG diet represent a new accelerated model of dry AMD, and, LG diet represents a potential therapeutic intervention to limit risk for or progress of AMD.

Materials and Methods

Animals and diets:

Nrf2 +/- and Nrf2 -/- were obtained from Michael Freeman (Vanderbilt University) and Jackson Laboratories (Bar Harbor, ME) respectively, and were interbred to generate Nrf2 -/- mice.

Animals were fed standard chow ad libitum (Teklad 7012, Harlan Laboratories, Madison, WI) until 3-months of age, at which time they were placed on study diet. 39 Nrf2 -/- male mice were randomized into groups of 20 HG-fed mice and 19 LG-fed mice. Diets contained identical macronutrient compositions with the exception that the HG starch was composed of 100% amylopectin (Amioca starch, Ingredion Inc., Bridgewater, NJ), while the LG starch was composed of 70% amylose/30% amylopectin (Hylon VII starch, Ingredion Inc., Bridgewater, NJ)(16). Diet composition was 542 g/kg starch, 200 g/kg casein, 85 g/kg sucrose, 56 g/kg soybean oil, 50 g/kg wheat bran, 2 g/kg DL methionine, 10 g/kg vitamin mix, and 35 g/kg mineral mix. Macronutrient energy percentages were 65% carbohydrate, 21% protein, and 14% fat for both HG and LG diets. All diets were formulated by Bio-Serv (Frenchtown, NJ). Mice were group pair-fed to ensure equal consumption between diet groups.

Body composition analysis was performed at 13-months using a EchoMRI-700 to measure fat mass and lean body mass. At 18-months of age, mice were anesthetized with ketamine and xylazine, the fundus was photographed using a Micron III retinal microscope (Phoenix research labs, Pleasanton, CA), and fluorescein angiography images were acquired following intraperitoneal injection of fluorescein (Acorn). Mice were fasted for 6 hours and were subsequently killed. All animal work was performed at this center and approved by the Tufts University IACUC in adherence with the ARVO statement for the use of animals in ophthalmic and vision research. Animals deemed to be in poor health were euthanized and excluded from the analysis. In total, 16 Nrf2-null HG mice (Nrf2-HG) and 17 Nrf2-null LG mice (Nrf2-LG) were included in the final analysis. 5 Nrf2-HG and 4 Nrf2-LG mice were found to have liver tumors upon necropsy.

Intraperitoneal glucose tolerance test and Insulin measurement:

Intraperitoneal glucose tolerance tests (IPGTT) were performed at 10-months. Mice were fasted for 6 h before IPTGG. A clean razor blade was used to make a horizontal cut in the lateral tail vein, releasing about 5 µl of blood that was applied to a OneTouch® Ultra® test strip in a OneTouch® Ultra2® glucometer (Lifescan Inc., Milpitas, CA) to obtain fasting glucose levels. For the glucose tolerance test, each mouse was injected intraperitoneally with 1 g/kg body weight D-(+)-glucose (≥99.5%, Sigma, St. Louis, MO) via a #25-5/8 gauge syringe. At 15, 30, 60 and 120 min after injection, the tail vein cut in each mouse was moistened to remove the clot and dried before release of another 5 µl of blood. This blood was applied to the test strip in the glucometer to measure the blood glucose level.

Insulin was measured at 18-months from fasted plasma samples using the ultrasensitive mouse insulin ELISA kit, according to the manufacturer's instructions (Crystal Chem, Elk Grove Village, IL)

Transmission Electron Microscopy (EM) and Light Microscopy Analysis:

Eyes were removed and immediately fixed in EM fixative (2.5% glutaraldehyde, 2% paraformaldehyde, with 0.025% (w/v) CaCl₂ in 0.1M sodium cacodylate buffer, pH 7.4). Eyes were washed 2 x 10 min in 0.1M sodium cacodylate buffer containing 5% sucrose, post-fixed 3.5 h in 1% osmium tetroxide in 0.1M cacodylate buffer containing 2% sucrose, washed 1 x 10 min in buffer and 1 x 10 min in distilled water (DW), and held in 4% uranyl acetate 1 h in the dark. Samples were then washed 1 x 10 min in DW, dehydrated 2 x 15 min each in graded ethanols (30%-100%) and propylene oxide, infiltrated in Embed-812 resin (Electron Microscopy Sciences, Hatfield, PA) for 24 on a rotator, and polymerized at 70 °C for 48 h. Sectioning was performed on a Leica EM UC7 Ultracut microtome using diamond knives (Diatome, Hatfield, PA). Semi-thin (0.5 µm) sections were stained with 1% toluidine blue in 1% sodium borate. Thin (silver) sections were collected on copper 135 hex grids, post-stained with 4% uranyl acetate in 50% (aq.) methanol and Reynold's lead citrate, and then viewed and photographed using a JEOL 1200 transmission electron microscope. Sections were photographed at 1mm from the optic nerve head. For semi-quantitative analysis of EM features, 35 20000X images were evaluated from 8-9 different eyes per group and parameters were then summarized per 100 µm of linear Bruch's membrane.

For light microscopy, semi-thin toluidine blue stained sections were photographed on an Olympus photomicroscope equipped with a digital camera. For morphometric analysis of RPE, 60x magnification images were taken from independent sections of each eye. Images were taken approximately 1 mm from the optic nerve head, on the same side as where TEM images were photographed. Quantification was performed using ImageJ software (NIH), setting thresholds for pigmentation based on the red channel. Each section had a contiguous RPE stretch of 291 µm. For quantification of the outer nuclear layer, measurements were taken every 250 µm from the optic nerve head on superior and inferior hemispheres. These were averaged from two independent sections of each eye; 10-11 different eyes per group. The retina damage score was computed by calculating the inverse of the area under the ONL thickness curve, and scaling the results, such that 24-month wildtype LG-fed mice had a score of zero, as we did previously (17).

Immunofluorescence and immunohistochemistry:

Enucleated eyes were immediately fixed in 4% paraformaldehyde for 1 hr. at 4 °C and transferred to PBS. The cornea and lens were removed, and the remaining eye cup was transferred to 30% sucrose for cryopreservation and then embedded in OCT. Cryosections were obtained at a thickness of 12 µm, dried overnight, and stored at -80°C.

For immunofluorescence, tissue sections were rehydrated in PBS containing 0.1% (v/v) Triton X-100 (PBT). For immunofluorescent detection of the RPE, slides were bleached using 10% hydrogen peroxide for 2 hrs. at 65°C. Next slides were blocked using normal donkey serum (Jackson Immunoresearch), incubated with primary antibodies for 2 hrs., washed with PBT, and incubated with appropriate secondary antibodies conjugated to either Cy3 or Alexa Fluor 488 (Jackson Immunoresearch). Slides were mounted in Prolong Gold Antifade with DAPI (Molecular Probes) and photographed on a Zeiss Axiovert fluorescence microscope and digital camera.

Primary antibodies and dilution:

<u>Species</u>	<u>ID</u>	<u>Dilution</u>	<u>Source</u>
Mouse	Anti-Nw-(carboxyethyl) arginine (CEA)	1:250	Ryoji Nagai
Rabbit	Anti-Glucosepane	1:200	David Spiegel

Rabbit	Anti-Superoxide dismutase 1 (SOD1)	1:500	Sigma
Rabbit	GCLM (Glutamate-Cysteine Ligase Modifier Subunit)	1:500	Abcam
Rabbit	Glyoxalase 1 (GLO1)	1:2000	Casper Schalkwijk (35)

Isolectin B4 staining was performed by incubating sections with Biotinylated Griffonia Simplicifolia Lectin I isolectin B4 (Vector Laboratories) followed by detection using Alexa Fluor 488-conjugated streptavidin (Invitrogen).

Statistical Analyses:

For univariate analyses, data were evaluated using either SPSS (IBM) or Microsoft Excel. First, data was evaluated as to whether it fit in a normal distribution or not, based on kurtosis and skewness. Pair-wise data that fit in a normal distribution was analyzed by a 2-tailed Student's t-test followed by an F-test to determine if the samples have equal variance. If the data did not fit a normal distribution, it was evaluated for pairwise comparisons using Wilcoxon Mann-Whitney U test. Correlation analysis was performed in SPSS using Pearson correlation. Analyses for gene-diet interactions was performed in SPSS as a univariate general linear model using a Type III sum-of-squares method.

Determination of protein glycation, oxidation and nitration adducts:

Targeted metabolomics was determined by stable isotopic dilution analysis liquid chromatography-tandem mass spectrometry (LC-MS/MS) by the protocol previously described (55). Analytes determined were: N_ε-fructosyl-lysine (FL), N_ε-carboxymethyl-lysine (CML), N_ε-(1-carboxyethyl)lysine (CEL), methylglyoxal and 3-deoxyglucosone-derived hydroimidazolones (MG-H1 and 3DG-H, respectively), glucosepane, glutamic semialdehyde (GSA), 3-nitrotyrosine (3-NT), pentosidine, and related amino acids. Fasting plasma (10 μl) was diluted to 500 μl water and washed by diafiltration with 4-cycles of concentration to 50 μl and dilution to 500 μl with further aliquots of water. The resultant protein (50 μl) was delipidated by extraction 3 times with one-volume of water-saturated ether, the residual ether removed by centrifugal evaporation for 5 min under vacuum (20 mmHg) and the protein concentration determined by the Bradford method. An aliquot (100 μg protein) was then digested enzymatically by consecutive incubation with pepsin, pronase E and finally aminopeptidase with prolidase under argon over 4 days. Blanks and control digests of human serum albumin were performed concurrently to provide for protease autohydrolysis correction. Addition of thymol antioxidant and antibiotics after the neutralization step prevents artefactual oxidation and bacterial contamination. The process was performed aseptically and automatically by custom program in a CTC-PAL sample autoprocessor (CTC Analytics, Zwingen, Switzerland). Analytes were detected and quantified by stable isotopic dilution analysis electrospray positive ionization multiple reaction monitoring LC-MS/MS using an Acquity ultra high performance chromatography (UPLC) system with a Xevo-TQS tandem mass spectrometer. Chromatography was with two graphitic Hypercarb™ columns (5 μm particle size; column-1, 2 x 50 mm and column-2, 2 x 250 mm) with eluent 0.1% trifluoroacetic acid in water with a custom program for multi-step gradient of acetonitrile and column switching.

Results

In order to test whether diet can modulate ocular phenotypes in Nrf2-null mice, we fed male Nrf2-null mice calorically matched HG or LG diets, beginning at 12-weeks of life (simplified hereon as Nrf2-HG or Nrf2-LG). Food consumption was monitored and mice in HG or LG groups were given access to the same amount of food such that both groups consumed equal amounts of diets. They were killed at 18-months. Nrf2-HG mice gained weight and became obese, comparable to wildtype mice fed HG diets (WT-HG) (17, 56, 57), but different from Nrf2-null mice that are generally resistant to obesity when fed high-fat diets (58). In comparison, Nrf2-LG mice, like wildtype mice fed LG diets (WT-LG), remained lean throughout the study (Fig. 1A,B). Along with increased fat mass, Nrf2-HG mice were hyperglycemic and glucose intolerant, while Nrf2-LG mice maintained normal glycemia (Fig. 1C,D). Nrf2-HG mice had increased levels of fasting plasma insulin, indicating that they were insulin resistant (Fig. 1E).

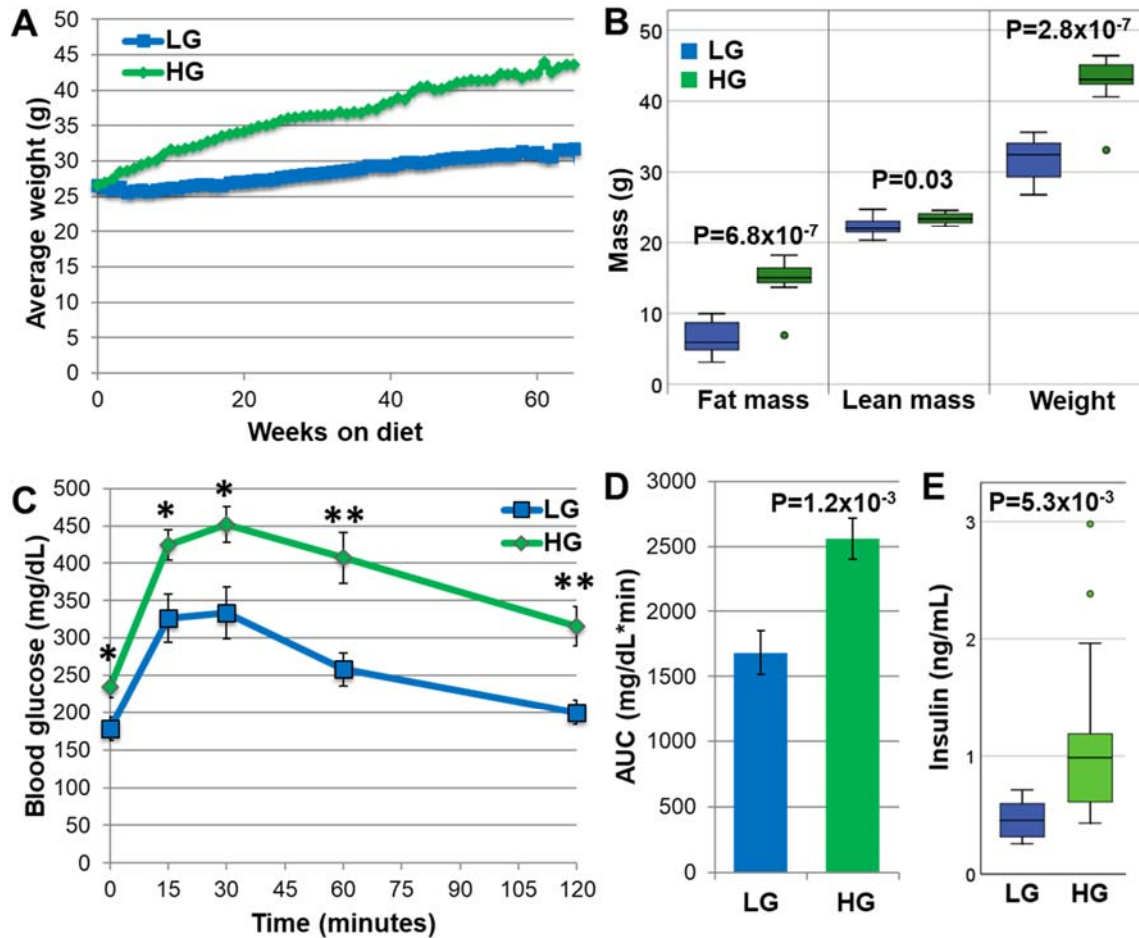


Figure 1. Nrf2-HG mice develop obesity, hyperglycemia, and glucose intolerance. **(A)** The average body weight of Nrf2-HG mice increased 35% Nrf2-LG mice with aging. **(B)** Body mass composition indicates that the increased body weight was from increased fat mass and not lean body mass. **(C)** Intraperitoneal glucose tolerance tests indicate that Nrf2-HG mice have significantly increased fasting blood glucose and impaired glucose tolerance relative to Nrf2-LG mice. **(D)** Quantitation of the area under the curve for the glucose tolerance test indicates 52% increased AUC for Nrf2-HG mice. **(E)** Fasting insulin levels were increased 148% in Nrf2-HG mice. Data points indicate means and error bars indicate SEM. All statistical tests performed were Student's T-tests: *, $P < 0.05$; **, $P < 0.01$. Sample size is $n = 20$ (HG), $n = 19$ (LG) in **(A)**; $n = 10$ (HG), $n = 12$ (LG) in **(B)**; $n = 11$ in **(C,D)**; $n = 14$ in **(E)**

In order to assess effects of glycemia on retinal health of Nrf2-null mice fed HG or LG diets, we performed histological analysis of retinas from 18-month old mice. First, we compared Nrf2-null mice fed HG or LG diets to WT mice fed identical diets (17). WT-LG or Nrf2-LG mice had intact, normally laminated retinas and a typical monolayered RPE (Fig. 2A,B). 18-month WT-HG mice also had grossly normal retinal lamination and structure (Fig. 2C), although quantitative studies did reveal mild thinning of the ONL (Fig. 2I). In comparison, Nrf2-HG mice presented with many retinal abnormalities, including a dramatic thinning of the ONL (Fig. 2D-F, I) and atrophy of the RPE (Fig. 2D-F). RPE atrophy was observed both localized (Fig. 2D, F) or more broadly (Fig. 2E) and was often associated with more dramatically thinned ONL. Some Nrf2-HG retinas developed large drusenoid deposits that displaced the RPE and overlying photoreceptors (Fig. 2F). We also observed detachment of

the RPE from Bruch's membrane (Fig. 2G,H), hypopigmentation of the RPE (Fig. 2H) and even hyperplasia of the RPE (Fig. 2H) in *Nrf2*-HG retinas. Together, the retinal phenotypes observed in *Nrf2*-HG mice resemble those seen in dry AMD in humans.

In order to better quantify phenotypic changes and variance, we quantified ONL thickness across the whole retina in 18-month WT and *Nrf2*-null mice fed HG or LG diets (Fig. 2I). In both genotypes, HG-fed mice had thinner ONLs than LG-fed mice and *Nrf2*-null mice had thinner ONLs than WT mice. To more easily relate ONL thinning to other parameters, we computed a retinal damage score, calculated as the inverse of the area under the ONL thickness curve (Fig. 2J and (17), see methods). Consistent with the crucial protective role of *Nrf2*, both diet groups of *Nrf2*^{-/-} mice had higher retinal damage scores than WT-LG mice (Fig. 2J). *Nrf2*-HG mice had retina damage scores that were significantly higher than WT-HG mice ($P=1.2 \times 10^{-5}$) and *Nrf2*-LG mice ($P=1.4 \times 10^{-6}$) (Fig. 2J). Strikingly, *Nrf2*-LG mice had retinal damage scores similar to those observed in WT-HG mice. On average 18-month *Nrf2*-HG retina damage scores were higher than 24-month WT-HG-fed mice (11.8 +/- 3.3 for *Nrf2*-HG and 6.4 +/- 3.9 for WT-HG (Fig. 2J and (17))). Using a general linear model, we found that diet and genotype were each significantly associated with retinal damage score (diet: $P=3.7 \times 10^{-9}$; genotype: $P=8.1 \times 10^{-8}$), but there was no gene-diet interaction ($P=0.56$).

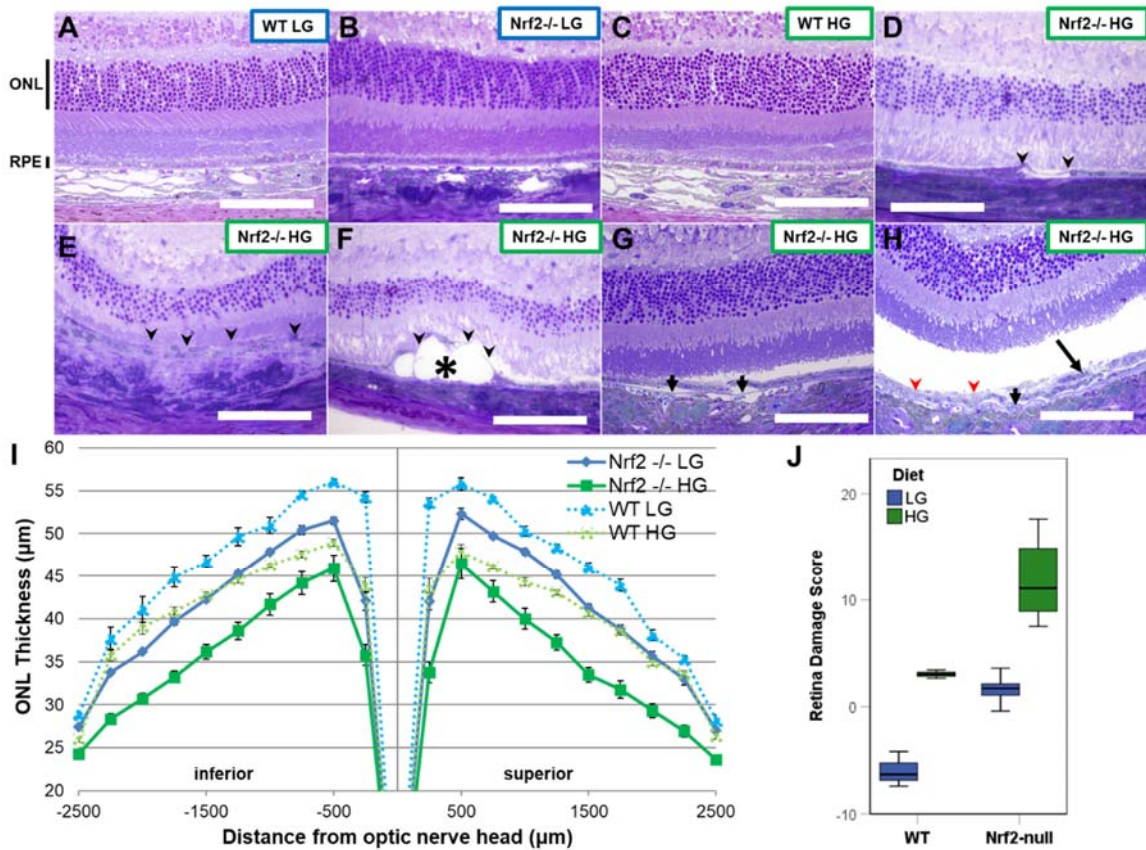


Figure 2. Nrf2-HG mice develop features of atrophic age-related macular degeneration. (**A-H**) Toluidine blue stained sections through the retinas of WT-LG (**A**), Nrf2-LG (**B**), and WT-HG (**C**), have normal architecture, whereas Nrf2-HG mouse retinas (**D-H**) show multiple lesions including: RPE atrophy (arrowheads), drusenoid deposits (asterisk), RPE detachments from Bruch's membrane (short arrows), hypopigmentation (red arrowheads), and multilayered RPE (long arrow). (**I**) Measurement of ONL thickness across the retinas of each dietary and genotype group indicates moderate thinning of WT-HG and Nrf2-LG ONL, but severe thinning of Nrf2-HG ONL relative to WT-LG ONL. (**J**) Boxplots of retina damage score, based on the area under the ONL thickness plot show increased retina damage score in Nrf2-HG mice compared to all other groups. Abbreviations: ONL – outer nuclear layer, RPE – retinal pigmented epithelium. Data points in (**I**) indicate means and error bars indicate SEM. Sample size is n=10 (Nrf2-HG), n=11 (Nrf2-LG), n=3 (WT) in (**I,J**). Scale bar is 100µm.

Another indicator of AMD in humans is pigmentary abnormalities, both hyper and hypopigmentation. We found that Nrf2-HG mice had broad areas of hypopigmentation as well as hyperpigmentation, whereas Nrf2-LG mice had more typical fundus appearances of 18-mo. mice (Figure 3A-D). Histological analysis of the RPE revealed overall quantitative hypopigmentation of Nrf2-HG RPE (Figure 3E-H), as well as RPE thinning and atrophy (Figure 3E,F, I, J). We observed a linear relationship between RPE hypopigmentation or RPE thinning and retina damage score (Figure 3H, J), consistent with the relationship between RPE dystrophy and photoreceptor degeneration that is seen in atrophic AMD in people. Within the Nrf2-LG group RPE area or pigment area varied but there was no statistically significant correlation of these values with retina damage score (Figure 3 H, J).

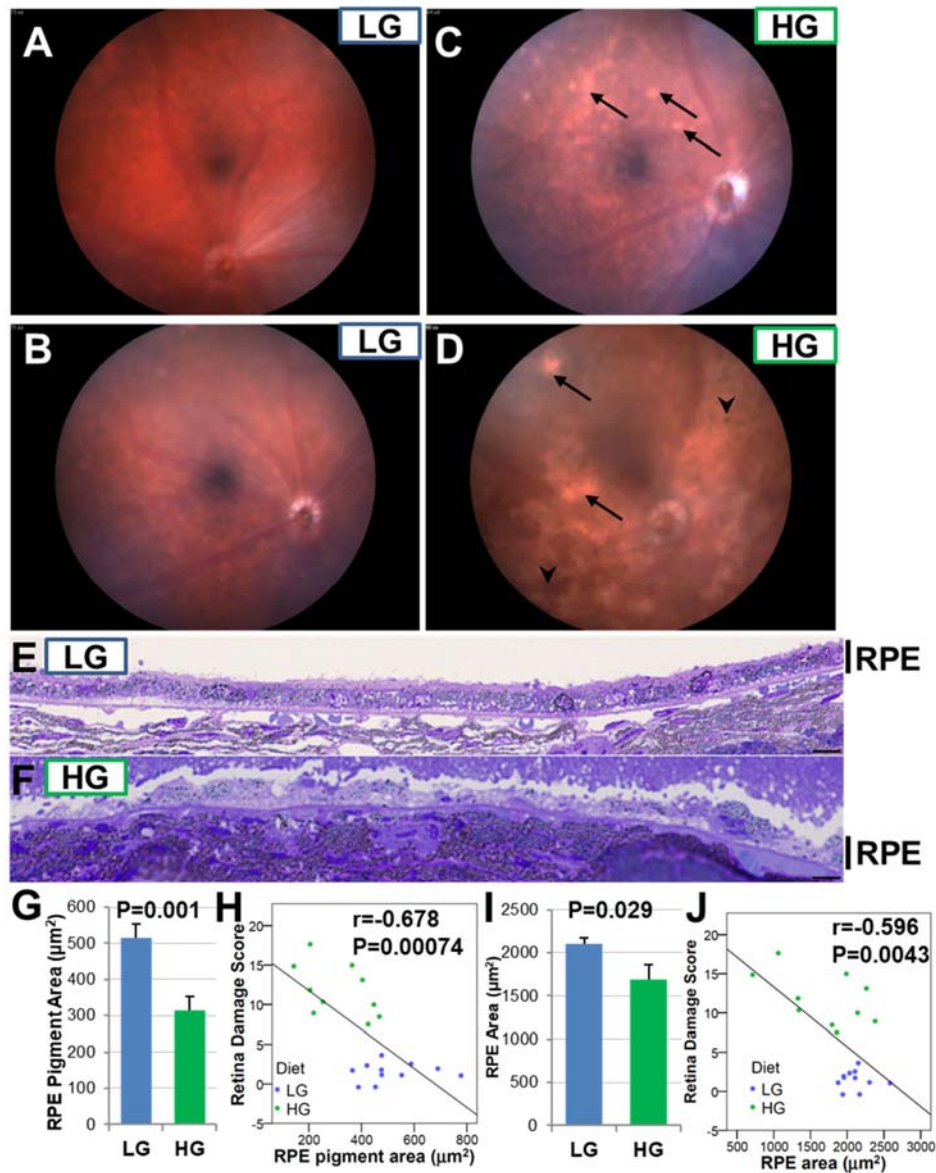


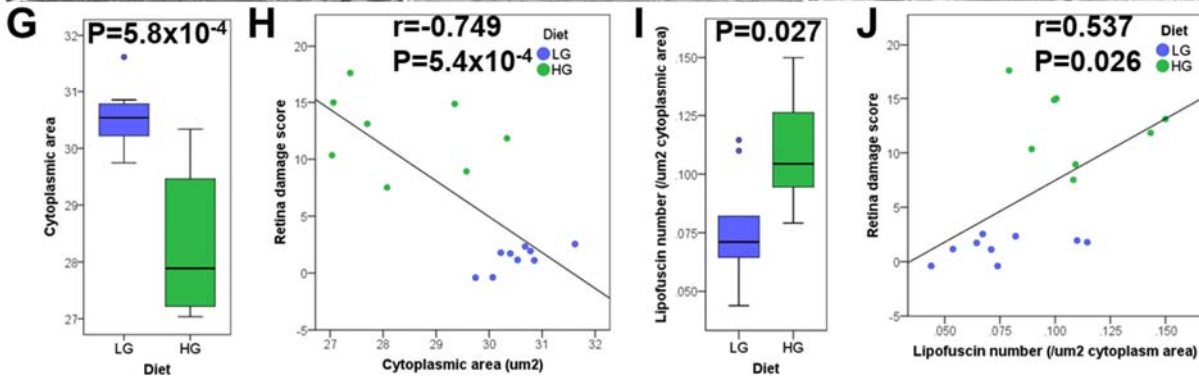
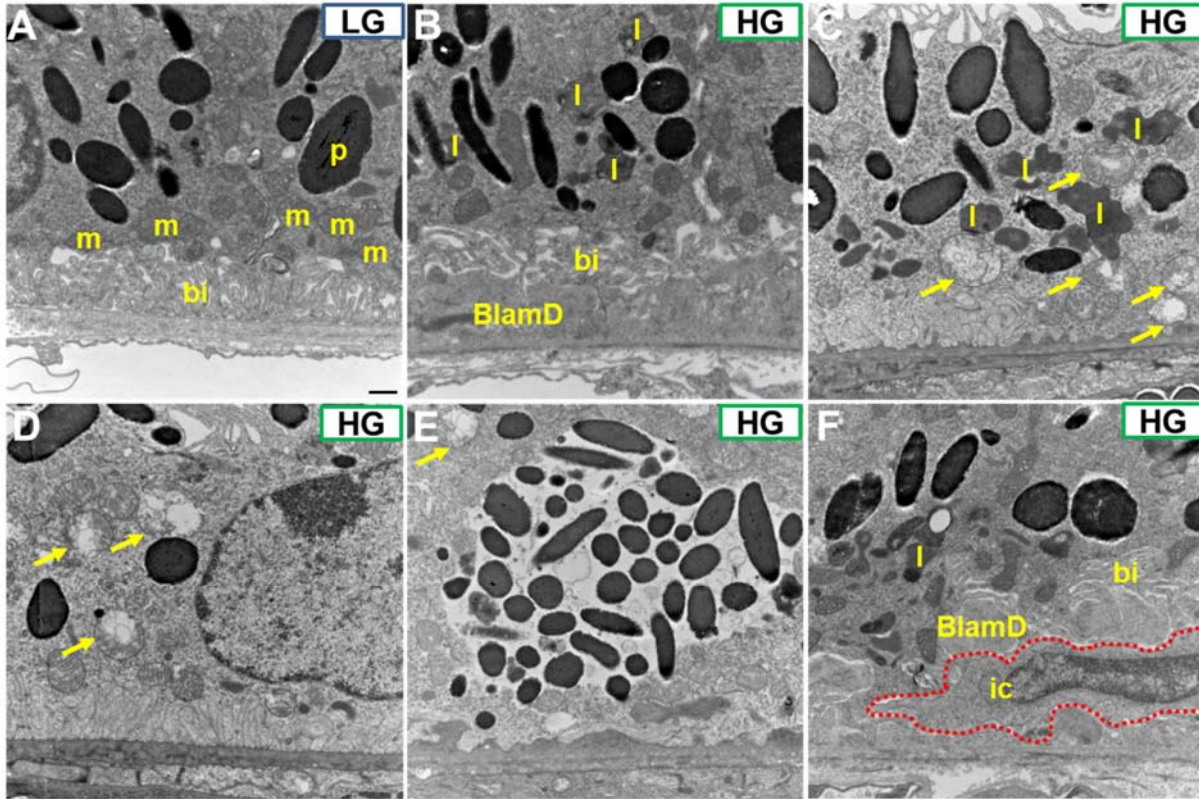
Figure 3. Nrf2-HG eyes develop pigment abnormalities and RPE thinning. (A-D) Fundus photographs show areas of hypopigmentation (arrows) and hyperpigmentation (arrowheads) in Nrf2-HG eyes. (E-F) Toluidine blue stained sections through the RPE show hypopigmentation and thinning of the Nrf2-HG RPE. (G-H) Quantitation of pigment granule area demonstrates hypopigmentation in Nrf2-HG RPE (G) that is negatively correlated with the retina damage score (H). (I-J) Quantitation of RPE area demonstrates thinning of the Nrf2-HG RPE (I) that is negatively correlated with the retina damage score (J). Bar graphs indicate means and error bars indicate SEM. Statistical tests performed were Student's T-test (G,I) or Pearson correlation (H,J). Sample size is n=10 (Nrf2-HG), n=11 (Nrf2-LG) in (G-J). Scale bar in (E,F) is 10 μ m.

Several additional hallmarks of AMD were visualized in electron micrographs (EM) of 18-mo. RPE. Nrf2-LG RPE often showed several large oblong pigment granules and intact mitochondria overlying the basal infoldings, similar to the appearance of WT LG-fed mice (Figure 4A, Supp. Figure 1) and healthy younger mice (59). In contrast, Nrf2-HG RPE had many AMD features, including large basal lamellar deposits (Figure 4B), accumulation of

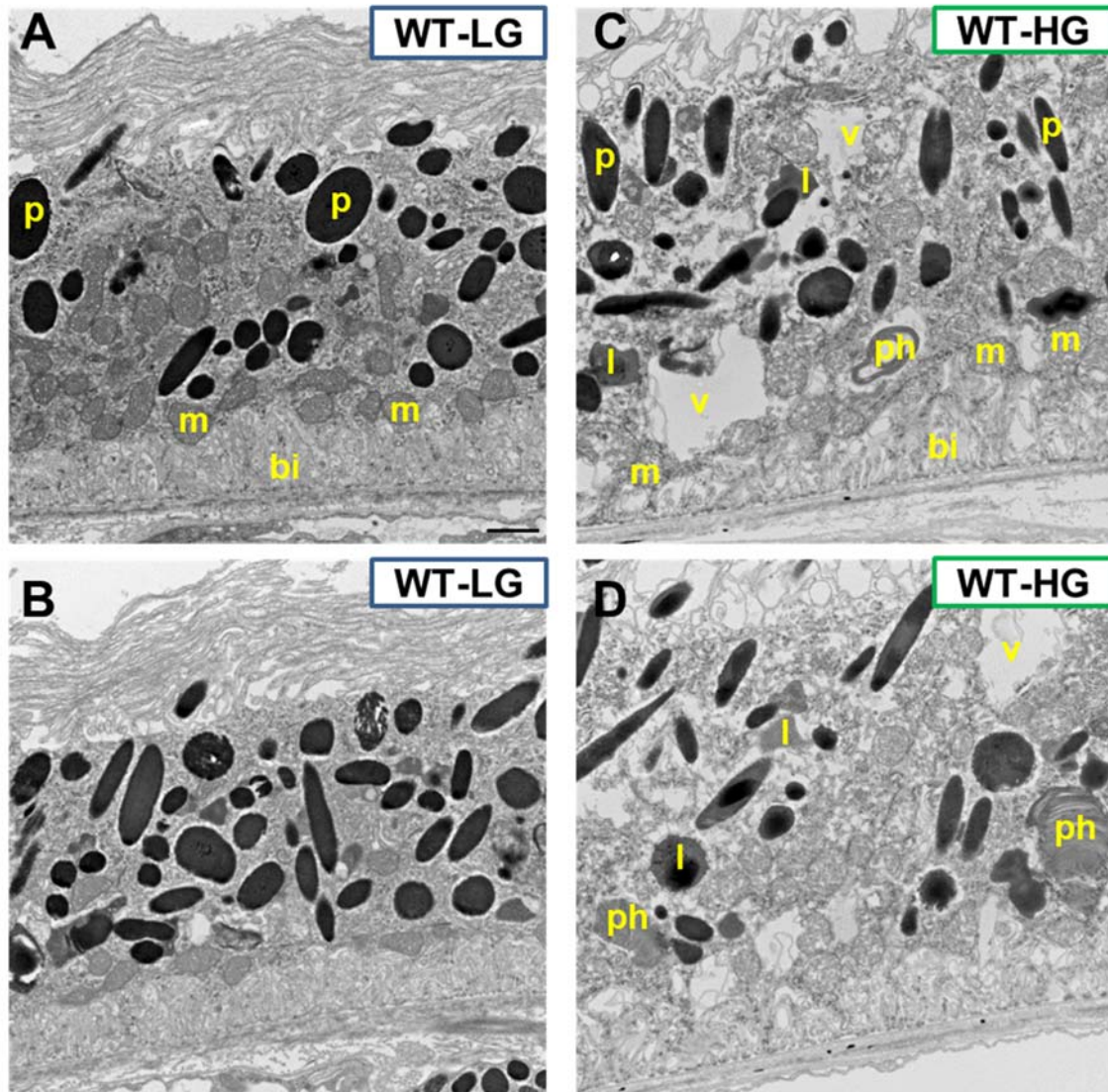
lipofuscin granules (Figure 4B, 4C, 4I), and loss or displacement of basal infoldings. Pigmentary abnormalities like those seen in fundus imaging and histologically were evident at the cellular level, where hypopigmentation (Figure 4D) and hyperpigmentation (Figure 4E) were observed. We also observed severe mitochondrial degeneration in Nrf2-HG RPE, as indicated by vacuolated and swollen mitochondria (Figure 4C-E). Finally, we occasionally observed infiltrating cells, likely macrophages, between the RPE plasma membrane and Bruch's membrane (Figure 4F).

In order to corroborate the findings above, we quantified cytosolic area and numbers of lipofuscin granules from Nrf2-null LG or Nrf2-null HG RPE EM images. As might be expected if cellular area is displaced by deposits or vacuoles, cytoplasmic area was quantitatively smaller in Nrf2-null HG RPE than Nrf2-LG RPE (Figure 4G), and negatively associated with retina damage score (Figure 4H). Lipofuscin granules were increased in Nrf2-null HG RPE (Figure 4I), and positively associated with retina damage score (Figure 4J). Increased lipofuscin granules and decreased cytoplasmic area was also observed in 18-mo. RPE from WT HG-fed (Supp. Figure 1).

Figure 4. Ultrastructural changes, mitochondrial degeneration, and lipofuscin accumulation in Nrf2-HG RPE. **(A-F)** Electron micrographs of RPE cells showing intact basal infoldings, mitochondria, and oblong pigment granule cells in Nrf2-LG RPE **(A)**, whereas Nrf2-HG RPE have missing or mislocalized basal infoldings **(B)**, accumulation of lipofuscin **(B, C, F)**, accumulation of basal laminar deposits **(B, F)**, swollen and degenerated mitochondria (arrows, **C-E**), hypopigmentation **(D)**, hyperpigmentation **(E)**, and infiltrating cells (red dashed line, **F**). **(G-H)** Boxplots indicate that Nrf2-HG RPE has reduced cytoplasmic area **(G)**, which is negatively correlated with retina damage score **(H)**. **(I-J)** Boxplots indicate that Nrf2-HG has increased numbers of lipofuscin granules **(I)**, which are positively correlated with retina damage score **(J)**. Abbreviations: bi-basal infoldings, BlamD-basal laminar deposits, ic-infiltrating cell, l-lipofuscin granule, m-mitochondria, p-pigment granule. Statistical tests performed were Student's T-test **(G,I)** or Pearson correlation **(H,J)**. Sample size is n=8 (Nrf2-HG), n=9 (Nrf2-LG). Scale bar in **(A)** is 500 nm.



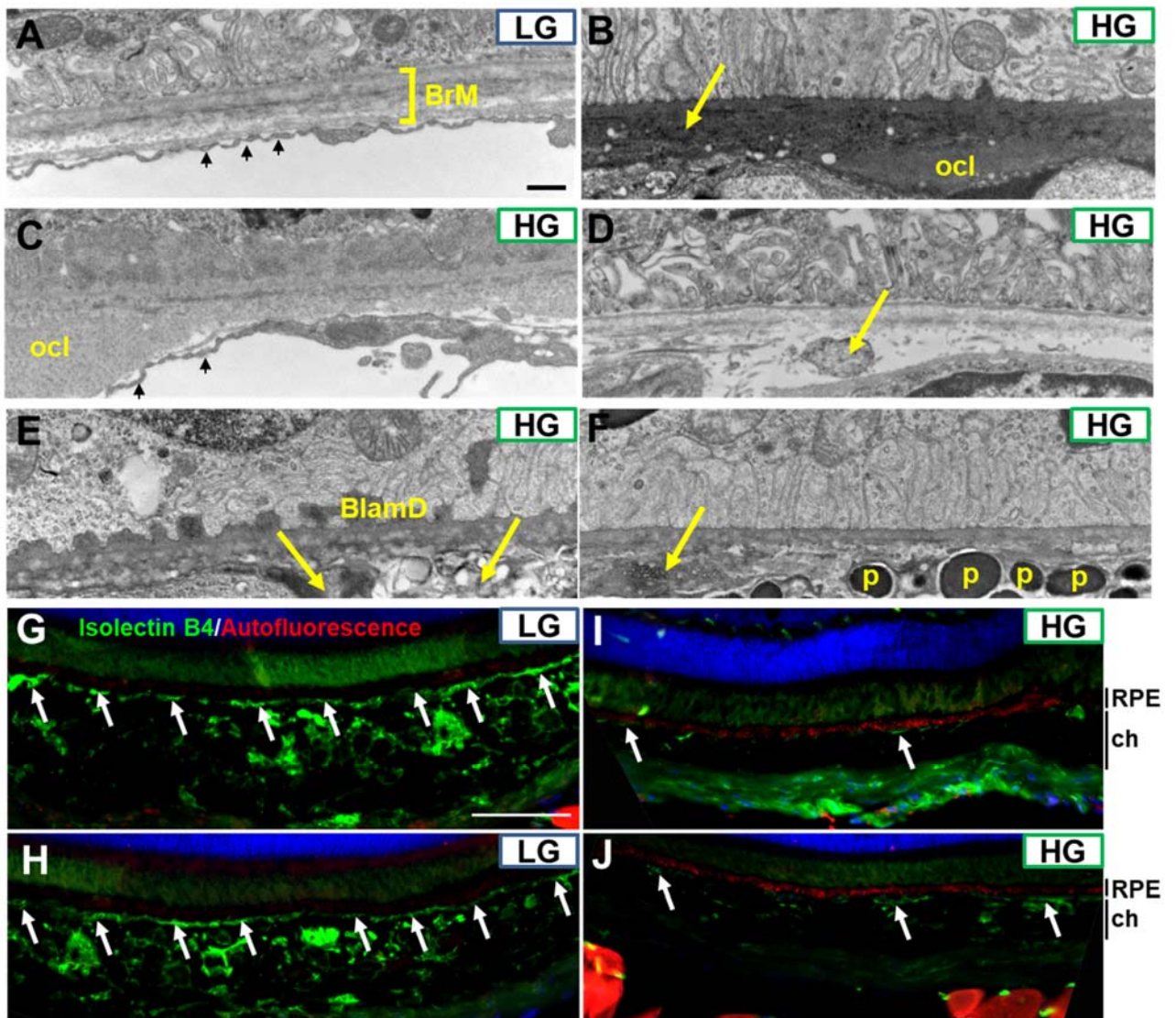
We also evaluated Bruch's membrane and the choriocapillaris. Nrf2-LG RPE had a normal pentalaminar Bruch's membrane and well-defined fenestrated choriocapillaris (Figure 5A) whereas Nrf2-HG RPE was associated with basal deposits, including outer collagenous layer deposits (Figure 5B-C), irregular and possibly lipidaceous deposits within Bruch's membrane (Figure 5D-F), and other deposits within Bruch's membrane, some of which resemble basal linear deposits (arrow, Figure 5B). We also observed frequent loss of the choriocapillaris and larger choroidal blood vessels in the Nrf2-HG eyes (Figure 5B, D-F), in some cases leading to the direct juxtaposition of the normally distally located choroidal melanocytes directly against Bruch's membrane (Figure 5F).



Supplementary Figure 1. Electron micrographs of 18-month WT-LG and WT-HG RPE. **(A,B)** WT-LG RPE is healthy, with intact basal laminar deposits, mitochondria, and pigment granules and resembles Nrf2-LG RPE. **(C,D)** WT-HG RPE shows some pathology like vacuoles, undigested phagosomes, and lipofuscin, but in contrast to Nrf2-HG RPE, has intact mitochondria and basal infoldings. Abbreviations: bi-basal infoldings, l-lipofuscin granule, m-mitochondria, p-pigment granule, ph-phagosome, v-vacuole. Scale bar in **(A)** is 500 nm.

We confirmed our EM-based analyses in sections from Nrf2-LG or Nrf2-HG eyes using Isolectin B4 to label blood vessels or autofluorescence as a surrogate for lipofuscin levels (Figure 5G-J). Nrf2-LG eyes showed intact choriocapillaris, large choroidal blood vessels, and minimal autofluorescence, whereas Nrf2-HG eyes exhibited large regions devoid of the choriocapillaris and choroidal blood vessels, as well as increased and punctate autofluorescence within the RPE (Figure 5I, J).

Taken together, our histological and ultrastructural characterizations of Nrf2-null eyes indicate that Nrf2-HG mice develop multiple, sometimes advanced, features of atrophic AMD, while Nrf2-LG mice do not develop notable AMD phenotypes.



Next we explored a molecular basis for the diet-imparted phenotypic differences between differences in Nrf2-LG and Nrf2-HG animals. Nrf2 functions as an anti-glycation factor by virtue of its activation of anti-oxidant pathways and its activation of the Glyoxalase 1 detoxification enzyme (Glo1). Consistent with these ascribed functions, Nrf2-null mice had twice the level of a major plasma AGE, MG-H1, relative to WT mice (Figure 6A).

Figure 5. Sub-RPE deposits, Bruch's membrane abnormalities, and loss of choriocapillaris in Nrf2-HG eyes. **(A-F)** Electron micrographs of the basal RPE, Bruch's membrane, and choriocapillaris indicate the lack of sub-RPE deposits, intact penta-laminar Bruch's membrane structure (square bracket in **A**), and well-fenestrated choriocapillaris (small arrows in **A**) in Nrf2-LG eyes (**A**). Nrf2-HG eyes contain multiple sub-RPE deposits, including outer collagenous layer deposits (**B,C**), basal laminar deposits (**E**), and other heterogeneous deposits (arrows in **B, D, E, F**). The choriocapillaris was largely absent except in a few areas (small arrows, **C**) and large choroidal blood vessels were absent and replaced by other choroidal tissues, including pigment granules (**F**). **(G-J)** Immunofluorescent staining for blood vessels via Isolectin B4 staining (green) or for autofluorescence (red) indicate intact choriocapillaris (arrows) and choroidal blood vessels in Nrf2-LG eyes (**G,H**) that are absent or degenerated in Nrf2-HG eyes (**I,J**), whereas autofluorescent puncta are highly increased in Nrf2-HG RPE (red staining in **I,J**). Abbreviations: BlamD-basal laminar deposit, BrM-Bruch's membrane, ch-choroid, ocl-outer collagenous layer deposit, p-pigment granule within melanocyte. Scale bar in **(A)** is 500nm; in **(G)** is 100 μ m.

Consistent with their being hyperglycemic, Nrf2-HG mice have higher plasma levels of pentosidine, a cross-linking AGE, and fructosyl-lysine, an early AGE product, than Nrf2-LG mice (Figure 6B,C).

We also assessed AGE accumulation in the retina. Two different kinds of AGES, N ω -(carboxyethyl)arginine (CEA), derived from methylglyoxal, and glucosepane, a cross-linking AGE, were both markedly increased in the RPE and choroid of Nrf2-HG mice (Figure 6D-H). Differences in levels of AGES were not clearly observed within the neural retina. Taken together, these data support the hypothesis that that Nrf2-LG RPE possesses increased capacity to detoxify or proteolytically remove AGES relative to Nrf2-HG RPE.

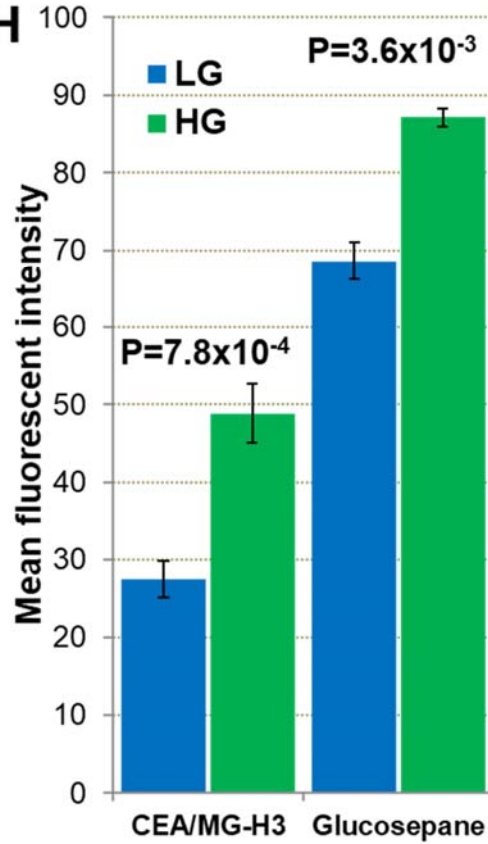
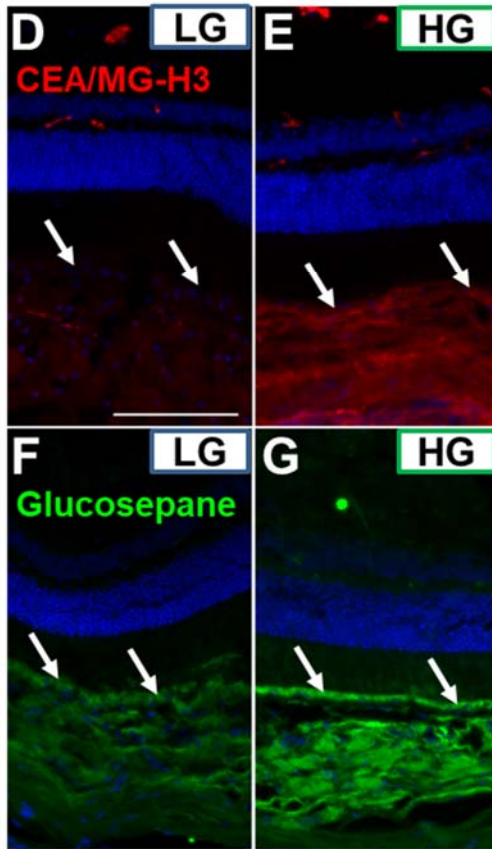
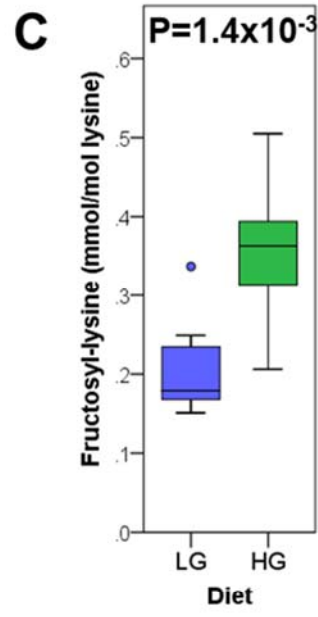
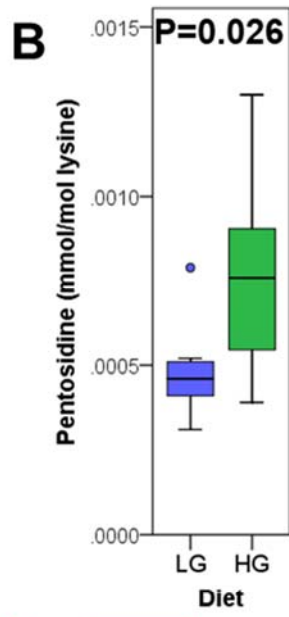
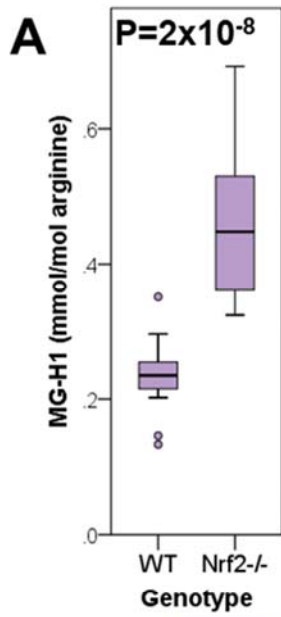
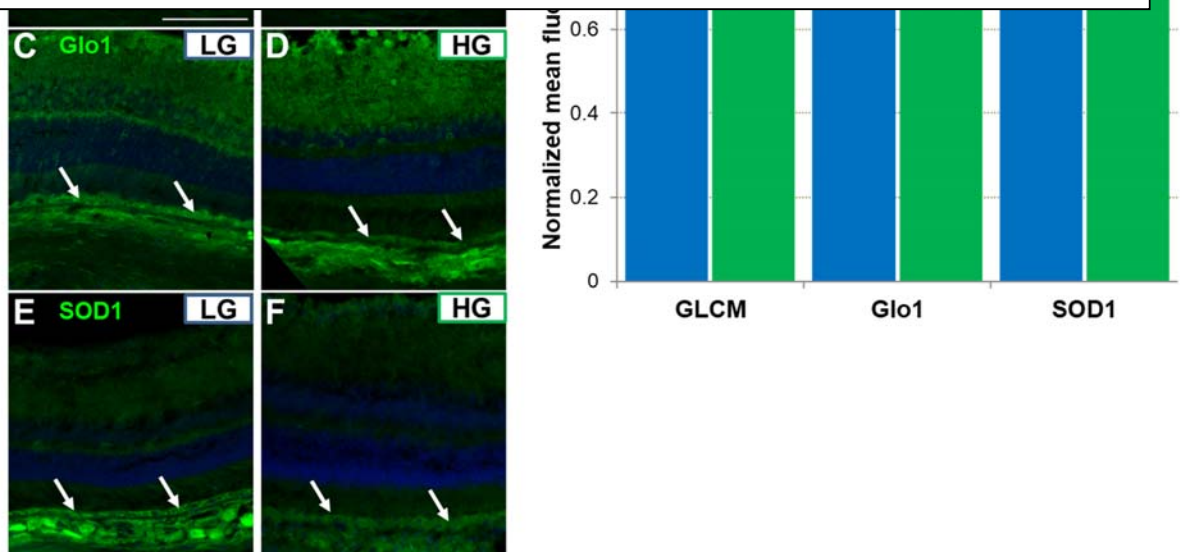


Figure 6. Accumulation of AGEs in the plasma and RPE of Nrf2-HG mice. **(A)** Plasma levels of MG-H1 are increased in the plasma of 18-mo. Nrf2-null mice relative to 24 mo. WT mice. **(B-C)** Plasma pentosidine and fructosyl-lysine are increased in the plasma of Nrf2-HG mice. **(D-G)** Immunofluorescent detection of CEA (red, **D,E**) and glucosepane (green, **F,G**) shows increased AGE levels in the RPE (arrows) and choroid in Nrf2-HG eyes. CEA is the more stable hydrolysis product of MG-H3. **(H)** Quantitation of fluorescent staining indicates statistically significant increases in CEA and glucosepane in the RPE of Nrf2-HG mice. Statistical tests performed were Student's T-test. Bars indicate mean and errors bars indicate SEM. Sample size is n=16 **(A)**, n=8 **(B-C)**, n=4 **(H)**. Scale bar in **(D)** is 100 μ m.

We hypothesized that antioxidant and antiglycative enzymes, even those that are direct transcription targets of Nrf2, may be upregulated in Nrf2-LG RPE. To test this hypothesis, we evaluated the levels of three different enzymes that are linked to Nrf2 - but may be regulated in Nrf2-independent pathways. Copper-Zinc Superoxide Dismutase 1 (SOD1) mitigates oxidative stress, Glo1 limits formation of the major glycating glucose metabolite MGO, and Glutamate-Cysteine Ligase Modifier Subunit (GCLM) is a rate-limiting protein in regulating synthesis of the major biological antioxidant glutathione. All three proteins showed modestly increased levels in Nrf2-LG RPE (Figure 7A-G).

Figure 7. Increased antioxidant and antiglycative potential of Nrf2-LG RPE. **(A-F)** Immunofluorescent detection of GCLM (A,B), Glo1 (C,D), or SOD1 (E,F) show increased staining in Nrf2-LG RPE (arrows). **(G)** Quantitation of fluorescent staining indicates statistically significant but modest relative increases in GCLM, Glo1, and SOD1 in Nrf2-LG RPE. Statistical tests performed were Student's T-test. Bars indicate mean and error bars indicate SEM. Sample size is n=4. Scale bar in **(A)** is 100 μ m.



Discussion

Given the dire need to combat the growing epidemic of AMD it is crucial to develop treatments against AMD, particularly the dry form, for which there are no remedies currently available. Our data establish Nrf2-HG mice as a new and potentially valuable model for

atrophic AMD, and suggest a dietary intervention to delay AMD phenotypes. Compared with WT-HG mice, which develop AMD phenotypes at 24-months, Nrf2-HG mice show more severe phenotypes that are obvious at 18-months. Many of these lesions approximate those of advanced dry AMD, such as geographic atrophy, loss of the choriocapillaris and photoreceptors, mitochondrial degeneration, and basal deposits. We also demonstrate the ability to limit these phenotypes via intake of an LG diet. The LG diet exploited here is attractive in that it is comparable to human diets that are rich in whole grains and high fiber, which protect from AMD (5-9). Our data can be compared to other gene-diet studies that modulated AMD outcomes using different levels of dietary fats, cholesterol, or protective gene variants compared to AMD-associated gene variants (18, 60-63).

The Nrf2-HG model may also be useful for exploring the role of the outer retinal vasculature in AMD. Imaging studies in human AMD have suggested that impaired choroidal blood flow precedes geographic atrophy (64). Furthermore, choriocapillaris degeneration is becoming better appreciated as a critical component of AMD and its progression to geographic atrophy (65). The RPE thinning and sub-RPE deposits, Bruch's membrane abnormalities, and loss of choriocapillaris in Nrf2-HG eyes suggest that the Nrf2-HG model should be useful for exploring the involvement of these tissues and the outer retinal vasculature in AMD and for testing drugs to preserve function of these tissues and cells. Longitudinal imaging studies, coupled with tissue-specific knockouts of Nrf2, can help with further pathomechanistic understanding.

Our observation of ultrastructural changes and apparent mitochondrial degeneration in Nrf2-null HG RPE (Fig. 4) indicate that the Nrf2-null HG mouse may also be a useful model to study the role of mitochondrial dysfunction in AMD. This is of growing interest since mitochondrial degeneration has been directly or indirectly connected to human AMD (66-69). Experiments that directly target mitochondrial function, like *in vivo* delivery of PGC1 α , or pharmaceutical mimetics to the RPE (70), may help elucidate the role of mitochondria in this AMD model.

What might be biochemical mechanisms by which the HG diet imparts damage to the retina?

The accumulation of cytotoxic AGEs in the RPE of Nrf2-HG mice may be a critical pathogenic mechanism explaining the observed RPE atrophy. Several different models could explain the AGE accumulation. A general explanation is that AGEs accumulate in Nrf2-HG mice due to the chronic hyperglycemia, leading to higher levels of AGE precursors in circulation. This hypothesis is supported by findings of higher levels of the AGE precursor fructosyl-lysine in the plasma of Nrf2-HG mice than Nrf2-LG mice and CEA/MG-H3 in the Nrf2-HG RPE (Figure 6). However, some other AGEs like MG-H1 were not increased in the plasma of Nrf2-HG mice. Another model invokes protective machineries, i.e. that Nrf2-LG RPE has enhanced machinery to detoxify AGE precursors or proteolytically remove AGEs. In addition to the data indicated above and prior precedent, this model is supported by the finding of higher levels of Glo1, SOD1, and GCLM in the Nrf2-LG RPE (Figure 7). Data from our group and others suggests that activation of protein quality control pathways like autophagy and the ubiquitin proteolysis system may facilitate removal of AGEs (24, 71-73). A corollary of this hypothesis is that upon aging and glycation stress, protective machineries are rendered less functional and/or insufficient to process the debris load that they encounter. Thus, damages and loss of function accrue at increasing rates. With limited antioxidant potential in a high glycaemic stress environment upon aging, the Nrf2-HG mouse typifies this, presenting features of AMD 6-months earlier than WT mice under the same conditions. The fact that we see differences in antioxidant enzymes and AGEs primarily in the RPE, corroborates decades of research indicating that the RPE is the processing site

and final repository of retinal debris. Understanding the mechanisms of AGE formation and clearance in the RPE may reveal novel targets for AMD.

Since the same salutary relationship is found upon feeding LG- versus HG diets to the Nrf2-null mice as is seen in WT mice, there appear to also be Nrf2-independent protective beneficial mechanisms that are reaped when consuming the LG diet. Metabolism is impacted by Nrf2 status and diet. Mice fed LG diets have higher levels of citric acid cycle intermediates like alpha ketoglutarate, fumarate, and malate, suggesting that LG diet may promote oxidative phosphorylation over glycolysis (17). Bioenergetics in the retina is tightly controlled to allow photoreceptors access to glucose to promote cell survival, while RPE cells largely rely on lactate for oxidative phosphorylation (74). In the RPE, dysregulated metabolism, for instance via activation of the mTORC1 pathway leads to RPE degeneration (75). RPE cells from AMD patients show altered bioenergetics, in particular reduced mitochondrial and glycolytic functions (69). This model is supported by the observation of improved RPE mitochondrial metabolism upon activation of AMPK signaling (76). LG diet, therefore, may act mimetically to metformin treatment to reduce glycemia and activate AMPK signaling.

Another mechanistic possibility recalls the relationship between diet, microbiota, and the gut. The LG diet is known to affect the composition of gut microbiota (17). The gut microbial ecosystem is associated with, and may lead to reduced systemic and inflammation (77), an established contributor to AMD pathogenesis (78-80). This appears to be attenuated in mice that consume the LG diet. Altered gut bacteria have also been reported in AMD (81). Nrf2-null mice have impaired gut barrier function, leading to bacterial endotoxin translocation across the gut (82). Hyperglycemic mice have similar phenotypes (83). Thus LG diet may enhance gut barrier function via effects on both microbiota composition and restoration of glycemic control. Other natural compounds that can activate the Nrf2 pathway, including the microbial metabolite urolithin A, derived from polyphenol-rich berries, or sulforaphane, a derivative of glucoraphanin that is found at high levels in cruciferous vegetables similarly improve gut barrier function (84, 85). Direct injection of sulforaphane into the blood of mice or dietary consumption of glucoraphanin-rich broccoli sprout extract has been shown to improve metabolism and protect against diabetes (86). Therefore, pathways that can exploit Nrf2 or its functionality represent promising interventional targets to treat disease, particularly age-related diseases, where function of Nrf2 diminishes with age and oxidative stresses increase (20, 54).

Our work also expands knowledge about Nrf2-dependent functions in the eye and elsewhere. For example, the loss of photoreceptors cells in Nrf2-LG mice beyond what is observed in 18-month WT-LG mice (Figure 2) or 24-month WT-LG mice (17), indicates diet-independent functions of Nrf2 in the eye. Similarly, Nrf2-HG mice developed AMD phenotypes beyond what is observed in WT-HG mice. Other diet-independent Nrf2-dependent phenotypes include liver cirrhosis and hepatocellular carcinoma (see Methods). We also defined diet-related phenotypes that were Nrf2-independent. These include effects of the HG diet on body weight and glucose tolerance (Figure 1). The development of obesity and insulin resistance in Nrf2-null HG mice is somewhat surprising, since Nrf2-null mice have been reported to be resistant to diet-induced obesity (58). HG-induced obesity is preceded by impaired fat oxidation, which leads to elevated lipogenesis in the liver, increased insulin secretion, and further obesity (57, 87), a mechanism that is Nrf2-independent. The combination of Nrf2-independent and diet-independent functions in this animal model explains in part the lack of a clear gene-diet interaction and suggests benefits for optimizing both diet and enhancement of Nrf2 function in human populations.

In summary, our work indicates that the Nrf2-HG mouse is a new, accelerated, model of atrophic AMD that provides opportunities to define critical pathogenic mechanisms for AMD development and timing windows for pharmaceutical or nutritional interventions. We describe one particularly promising intervention, the LG diet. Nrf2-LG mice had enhanced detoxification machinery in their RPE and were resistant to retinopathy described in Nrf2-null mice fed either regular diets or HG diets. The data presented also corroborate a significant body of prior laboratory investigation and human epidemiologic data that indicate that favoring LG carbohydrates over HG carbohydrates in the diet may provide an achievable, low-cost way to prolong retina function. That consuming low LG diets can limit the earliest indicators of AMD suggests that similar diets can be useful to delay compromises of vision that are coincident with AMD. Optimizing Nrf2 or its functionality represent additional promising targets to treat age-related diseases, where function of Nrf2 diminishes with age and oxidative stresses increase (20, 54).

Acknowledgements

We are grateful to Jennifer Cho and Jonathan Morrison for assistance with animal feeding, Barbara Nagel for histological and electron microscopy, Maria Stewart of Ingredion Inc. for dietary starches, Michael Freeman and Swati Biswas for Nrf2 +/- mice, and David Spiegel, Matthew Streeter, Ryoji Nagai, and Casper Schalkwijk for antibodies. Use of the EchoMRI-700 was supported by the Boston Nutrition Obesity Research Center (BNORC). Funding was supported by NIH RO1EY021212 and RO1EY028559 (to AT), USDA NIFA 2015-05470 (to AT and SR), The Thome Medical Foundation, and the Stanley N. Gershoff scholarship (to KMS). This material is based upon work supported by the U.S. Department of Agriculture – Agricultural Research Service (ARS), under Agreement No. 58-1950-4-003 (to AT). The authors declare no competing financial interests.

1. Age-Related Eye Disease Study 2 Research Group. Lutein + zeaxanthin and omega-3 fatty acids for age-related macular degeneration: the Age-Related Eye Disease Study 2 (AREDS2) randomized clinical trial. *JAMA* 2013;309:2005-15.
2. Sobrin L, Seddon JM. Nature and nurture- genes and environment- predict onset and progression of macular degeneration. *Prog Retin Eye Res*. 2014;40:1-15. doi: 10.1016/j.preteyeres.2013.12.004. PubMed PMID: 24374240.
3. Weikel KA, Chiu CJ, Taylor A. Nutritional modulation of age-related macular degeneration. *Molecular aspects of medicine*. 2012;33(4):318-75; PMID: PMC3392439.
4. Chiu CJ, Milton RC, Klein R, Gensler G, Taylor A. Dietary compound score and risk of age-related macular degeneration in the age-related eye disease study. *Ophthalmology*. 2009;116(5):939-46. PubMed PMID: 19410952.
5. Merle BMJ, Colijn JM, Cougnard-Gregoire A, de Koning-Backus APM, Delyfer MN, Kiefte-de Jong JC, Meester-Smoor M, Feart C, Verzijden T, Samieri C, Franco OH, Korobelnik JF, Klaver CCW, Delcourt C, Consortium E-R. Mediterranean Diet and Incidence of Advanced Age-Related Macular Degeneration: The EYE-RISK Consortium. *Ophthalmology*. 2019;126(3):381-90. doi: 10.1016/j.ophtha.2018.08.006. PubMed PMID: 30114418.
6. Chiu CJ, Chang ML, Zhang FF, Li T, Gensler G, Schleicher M, Taylor A. The relationship of major American dietary patterns to age-related macular degeneration. *American journal of ophthalmology*. 2014;158(1):118-27 e1. doi: 10.1016/j.ajo.2014.04.016. PubMed PMID: 24792100; PMID: 4101985.

7. Hogg RE, Woodside JV, McGrath A, Young IS, Vioque JL, Chakravarthy U, de Jong PT, Rahu M, Seland J, Soubrane G, Tomazzoli L, Topouzis F, Fletcher AE. Mediterranean Diet Score and Its Association with Age-Related Macular Degeneration: The European Eye Study. *Ophthalmology*. 2017;124(1):82-9. Epub 2016/11/09. doi: 10.1016/j.ophtha.2016.09.019. PubMed PMID: 27825655.
8. Kaushik S, Wang JJ, Flood V, Tan JS, Barclay AW, Wong TY, Brand-Miller J, Mitchell P. Dietary glycemic index and the risk of age-related macular degeneration. *Am J Clin Nutr*. 2008;88(4):1104-10. PubMed PMID: 18842800; PMCID: PMID18842800.
9. de Koning-Backus APM, Buitendijk GHS, Kiefte-de Jong JC, Colijn JM, Hofman A, Vingerling JR, Haverkort EB, Franco OH, Klaver CCW. Intake of Vegetables, Fruit, and Fish is Beneficial for Age-Related Macular Degeneration. *American journal of ophthalmology*. 2019;198:70-9. doi: 10.1016/j.ajo.2018.09.036. PubMed PMID: 30312575.
10. Chiu CJ, Klein R, Milton RC, Gensler G, Taylor A. Does eating particular diets alter risk of age-related macular degeneration in users of the age-related eye disease study supplements? *The British journal of ophthalmology*. 2009;1241-6. PubMed PMID: 19508997.
11. Chong EW, Simpson JA, Robman LD, Hodge AM, Aung KZ, English DR, Giles GG, Guymer RH. Red meat and chicken consumption and its association with age-related macular degeneration. *Am J Epidemiol*. 2009;169(7):867-76. PubMed PMID: 19234096.
12. Chiu CJ, Milton RC, Klein R, Gensler G, Taylor A. Dietary carbohydrate and the progression of age-related macular degeneration: a prospective study from the Age-Related Eye Disease Study. *Am J Clin Nutr*. 2007;86(4):1210-8. PubMed PMID: 17921404.
13. Chiu CJ, Hubbard LD, Armstrong J, Rogers G, Jacques PF, Chylack J, L. T., Hankinson SE, Willett WC, Taylor A. Dietary glycemic index and carbohydrate in relation to early age-related macular degeneration. *Am J Clin Nutr*. 2006;83:880-6. PubMed PMID: 16600942.
14. Leung IY, Sandstrom MM, Zucker CL, Neuringer M, Snodderly DM. Nutritional manipulation of primate retinas, II: effects of age, n-3 fatty acids, lutein, and zeaxanthin on retinal pigment epithelium. *Invest Ophthalmol Vis Sci*. 2004;45(9):3244-56. PubMed PMID: 15326147.
15. McGill TJ, Renner LM, Neuringer M. Elevated Fundus Autofluorescence in Monkeys Deficient in Lutein, Zeaxanthin, and Omega-3 Fatty Acids. *Invest Ophthalmol Vis Sci*. 2016;57(3):1361-9. Epub 2016/03/24. doi: 10.1167/iovs.15-18596. PubMed PMID: 27002296; PMCID: PMC4811180.
16. Weikel KA, Fitzgerald P, Shang F, Caceres MA, Bian Q, Handa JT, Stitt AW, Taylor A. Natural history of age-related retinal lesions that precede AMD in mice fed high or low glycemic index diets. *Invest Ophthalmol Vis Sci*. 2012;53(2):622-32; PMCID: PMC3317410.
17. Rowan S, Jiang S, Korem T, Szymanski J, Chang ML, Szelog J, Cassalman C, Dasuri K, McGuire C, Nagai R, Du XL, Brownlee M, Rabbani N, Thornalley PJ, Baleja JD, Deik AA, Pierce KA, Scott JM, Clish CB, Smith DE, Weinberger A, Avnit-Sagi T, Lotan-Pompan M, Segal E, Taylor A. Involvement of a gut-retina axis in protection against dietary glycemia-induced age-related macular degeneration. *Proc Natl Acad Sci U S A*. 2017;114(22):E4472-E81. Epub 2017/05/17. doi: 10.1073/pnas.1702302114. PubMed PMID: 28507131; PMCID: 5465926.
18. Malek G, Johnson LV, Mace BE, Saloupis P, Schmechel DE, Rickman DW, Toth CA, Sullivan PM, Bowes Rickman C. Apolipoprotein E allele-dependent pathogenesis: a model for age-related retinal degeneration. *Proc Natl Acad Sci U S A*. 2005;102(33):11900-5. PubMed PMID: 16079201.
19. Toomey CB, Kelly U, Saban DR, Bowes Rickman C. Regulation of age-related macular degeneration-like pathology by complement factor H. *Proc Natl Acad Sci U S A*. 2015;112(23):E3040-9. doi: 10.1073/pnas.1424391112. PubMed PMID: 25991857; PMCID: 4466717.
20. Bonilha VL, Bell BA, Rayborn ME, Samuels IS, King A, Hollyfield JG, Xie C, Cai H. Absence of DJ-1 causes age-related retinal abnormalities in association with increased oxidative stress. *Free radical biology & medicine*. 2017;104:226-37. Epub 2017/01/16. doi: 10.1016/j.freeradbiomed.2017.01.018. PubMed PMID: 28088625; PMCID: PMC5328840.
21. Mitter SK, Song C, Qi X, Mao H, Rao H, Akin D, Lewin A, Grant M, Dunn W, Jr., Ding J, Bowes Rickman C, Boulton M. Dysregulated autophagy in the RPE is associated with increased susceptibility

- to oxidative stress and AMD. *Autophagy*. 2014;10(11):1989-2005. Epub 2014/12/09. doi: 10.4161/autophagy.36184. PubMed PMID: 25484094; PMCID: 4502658.
22. Brown EE, DeWeerd AJ, Ildefonso CJ, Lewin AS, Ash JD. Mitochondrial oxidative stress in the retinal pigment epithelium (RPE) led to metabolic dysfunction in both the RPE and retinal photoreceptors. *Redox biology*. 2019;24:101201. Epub 2019/05/01. doi: 10.1016/j.redox.2019.101201. PubMed PMID: 31039480; PMCID: PMC6488819.
23. Fujihara M, Bartels E, Nielsen LB, Handa JT. A human apoB100 transgenic mouse expresses human apoB100 in the RPE and develops features of early AMD. *Experimental eye research*. 2009;88(6):1115-23. Epub 2009/05/20. doi: S0014-4835(09)00031-1 [pii] 10.1016/j.exer.2009.01.017. PubMed PMID: 19450445; PMCID: 2729121.
24. Uchiki T, Weikel KA, Jiao W, Shang F, Caceres A, Pawlak DB, Handa JT, Brownlee M, Nagaraj R, Taylor A. Glycation-altered proteolysis as a pathobiologic mechanism that links dietary glycemic index, aging, and age-related disease (in non diabetics). *Aging Cell*. 2012;11(1):1-13. Epub Nov 15 2011; PMCID: PMC3257376.
25. Crabb JW, Miyagi M, Gu X, Shadrach K, West KA, Sakaguchi H, Kamei M, Hasan A, Yan L, Rayborn ME, Salomon RG, Hollyfield JG. Drusen proteome analysis: an approach to the etiology of age-related macular degeneration. *Proc Natl Acad Sci U S A*. 2002;99(23):14682-7. PubMed PMID: 12391305; PMCID: PMC2722770.
26. Handa JT, Verzijl N, Matsunaga H, Aotaki-Keen A, Litty GA, te Koppele JM, Miyata T, Hjelmeland LM. Increase in the advanced glycation end product pentosidine in Bruch's membrane with age. *Invest Ophthalmol Vis Sci*. 1999;40:775-9.
27. Ishibashi T, Murata T, Hangai M, Nagai R, Horiuchi S, Lopez PF, Hinton DR, Ryan SJ. Advanced glycation end products in age-related macular degeneration. *Archives of ophthalmology*. 1998;116(12):1629-32. PubMed PMID: 9869793.
28. Howes KA, Liu Y, Dunaief JL, Milam A, Frederick JM, Marks A, Baehr W. Receptor for advanced glycation end products and age-related macular degeneration. *Invest Ophthalmol Vis Sci*. 2004;45(10):3713-20. Epub 2004/09/29. doi: 10.1167/iovs.04-0404. PubMed PMID: 15452081.
29. Ni J, Yuan X, Gu J, Yue X, Gu X, Nagaraj RH, Crabb JW. Plasma protein pentosidine and carboxymethyllysine, biomarkers for age-related macular degeneration. *Mol Cell Proteomics*. 2009;8(8):1921-33. Epub 2009/05/14. doi: M900127-MCP200 [pii] 10.1074/mcp.M900127-MCP200. PubMed PMID: 19435712; PMCID: PMC2722770.
30. Queisser MA, Yao D, Geisler S, Hammes HP, Lochnit G, Schleicher ED, Brownlee M, Preissner KT. Hyperglycemia impairs proteasome function by methylglyoxal. *Diabetes*. 2010;59(3):670-8; PMCID: PMC2828656.
31. Brown EE, Ball JD, Chen Z, Khurshid GS, Prosperi M, Ash JD. The Common Antidiabetic Drug Metformin Reduces Odds of Developing Age-Related Macular Degeneration. *Invest Ophthalmol Vis Sci*. 2019;60(5):1470-7. doi: 10.1167/iovs.18-26422. PubMed PMID: 30973575.
32. Tonelli C, Chio IIC, Tuveson DA. Transcriptional Regulation by Nrf2. *Antioxid Redox Signal*. 2018;29(17):1727-45. Epub 2017/09/14. doi: 10.1089/ars.2017.7342. PubMed PMID: 28899199; PMCID: PMC6208165.
33. Xue M, Momiji H, Rabbani N, Barker G, Bretschneider T, Shmygol A, Rand DA, Thornalley PJ. Frequency Modulated Translocational Oscillations of Nrf2 Mediate the Antioxidant Response Element Cytoprotective Transcriptional Response. *Antioxid Redox Signal*. 2014. Epub 2014/09/03. doi: 10.1089/ars.2014.5962. PubMed PMID: 25178584.
34. Xue M, Rabbani N, Momiji H, Imbasi P, Anwar MM, Kitteringham N, Park BK, Souma T, Moriguchi T, Yamamoto M, Thornalley PJ. Transcriptional control of glyoxalase 1 by Nrf2 provides a stress-responsive defence against dicarbonyl glycation. *The Biochemical journal*. 2012;443(1):213-22. PubMed PMID: 22188542.
35. Brouwers O, Niessen PM, Ferreira I, Miyata T, Scheffer PG, Teerlink T, Schrauwen P, Brownlee M, Stehouwer CD, Schalkwijk CG. Overexpression of glyoxalase-I reduces hyperglycemia-

induced levels of advanced glycation end products and oxidative stress in diabetic rats. *The Journal of biological chemistry*. 2011;286(2):1374-80; PMID: PMC3020745.

36. Giacco F, Du X, D'Agati VD, Milne R, Sui G, Geoffrion M, Brownlee M. Knockdown of glyoxalase 1 mimics diabetic nephropathy in nondiabetic mice. *Diabetes*. 2014;63(1):291-9. Epub 2013/09/26. doi: 10.2337/db13-0316. PubMed PMID: 24062246; PMID: PMC3868051.
37. Sanghvi VR, Leibold J, Mina M, Mohan P, Berishaj M, Li Z, Miele MM, Lailier N, Zhao C, de Stanchina E, Viale A, Akkari L, Lowe SW, Ciriello G, Hendrickson RC, Wendel HG. The Oncogenic Action of NRF2 Depends on De-glycation by Fructosamine-3-Kinase. *Cell*. 2019;178(4):807-19 e21. Epub 2019/08/10. doi: 10.1016/j.cell.2019.07.031. PubMed PMID: 31398338.
38. Pajares M, Jimenez-Moreno N, Garcia-Yague AJ, Escoll M, de Ceballos ML, Van Leuven F, Rabano A, Yamamoto M, Rojo AI, Cuadrado A. Transcription factor NFE2L2/NRF2 is a regulator of macroautophagy genes. *Autophagy*. 2016;12(10):1902-16. Epub 2016/07/19. doi: 10.1080/15548627.2016.1208889. PubMed PMID: 27427974; PMID: PMC5079676.
39. Holmstrom KM, Baird L, Zhang Y, Hargreaves I, Chalasani A, Land JM, Stanyer L, Yamamoto M, Dinkova-Kostova AT, Abramov AY. Nrf2 impacts cellular bioenergetics by controlling substrate availability for mitochondrial respiration. *Biol Open*. 2013;2(8):761-70. Epub 2013/08/21. doi: 10.1242/bio.20134853. PubMed PMID: 23951401; PMID: PMC3744067.
40. O'Mealey GB, Plafker KS, Berry WL, Janknecht R, Chan JY, Plafker SM. A PGAM5-KEAP1-Nrf2 complex is required for stress-induced mitochondrial retrograde trafficking. *Journal of cell science*. 2017;130(20):3467-80. Epub 2017/08/26. doi: 10.1242/jcs.203216. PubMed PMID: 28839075; PMID: PMC5665445.
41. Piantadosi CA, Carraway MS, Babiker A, Suliman HB. Heme oxygenase-1 regulates cardiac mitochondrial biogenesis via Nrf2-mediated transcriptional control of nuclear respiratory factor-1. *Circulation research*. 2008;103(11):1232-40. Epub 2008/10/11. doi: 10.1161/01.RES.0000338597.71702.ad. PubMed PMID: 18845810; PMID: PMC2694963.
42. Gureev AP, Shaforostova EA, Popov VN. Regulation of Mitochondrial Biogenesis as a Way for Active Longevity: Interaction Between the Nrf2 and PGC-1alpha Signaling Pathways. *Front Genet*. 2019;10:435. Epub 2019/05/30. doi: 10.3389/fgene.2019.00435. PubMed PMID: 31139208; PMID: PMC6527603.
43. Ramos-Gomez M, Kwak MK, Dolan PM, Itoh K, Yamamoto M, Talalay P, Kensler TW. Sensitivity to carcinogenesis is increased and chemoprotective efficacy of enzyme inducers is lost in nrf2 transcription factor-deficient mice. *Proc Natl Acad Sci U S A*. 2001;98(6):3410-5. Epub 2001/03/15. doi: 10.1073/pnas.051618798. PubMed PMID: 11248092; PMID: PMC30667.
44. Beyer TA, Xu W, Teupser D, auf dem Keller U, Bugnon P, Hildt E, Thiery J, Kan YW, Werner S. Impaired liver regeneration in Nrf2 knockout mice: role of ROS-mediated insulin/IGF-1 resistance. *EMBO J*. 2008;27(1):212-23. Epub 2007/12/07. doi: 10.1038/sj.emboj.7601950. PubMed PMID: 18059474; PMID: PMC2206132.
45. Cho HY, Jedlicka AE, Reddy SP, Kensler TW, Yamamoto M, Zhang LY, Kleeberger SR. Role of NRF2 in protection against hyperoxic lung injury in mice. *Am J Respir Cell Mol Biol*. 2002;26(2):175-82. Epub 2002/01/24. doi: 10.1165/ajrcmb.26.2.4501. PubMed PMID: 11804867.
46. Hubbs AF, Benkovic SA, Miller DB, O'Callaghan JP, Battelli L, Schwegler-Berry D, Ma Q. Vacuolar leukoencephalopathy with widespread astrogliosis in mice lacking transcription factor Nrf2. *Am J Pathol*. 2007;170(6):2068-76. Epub 2007/05/26. doi: 10.2353/ajpath.2007.060898. PubMed PMID: 17525273; PMID: PMC1899457.
47. Kansanen E, Kuosmanen SM, Leinonen H, Levonen AL. The Keap1-Nrf2 pathway: Mechanisms of activation and dysregulation in cancer. *Redox biology*. 2013;1(1):45-9. doi: 10.1016/j.redox.2012.10.001. PubMed PMID: 24024136; PMID: 3757665.
48. Wei Y, Gong J, Yoshida T, Eberhart CG, Xu Z, Kombairaju P, Sporn MB, Handa JT, Duh EJ. Nrf2 has a protective role against neuronal and capillary degeneration in retinal ischemia-reperfusion injury. *Free radical biology & medicine*. 2011;51(1):216-24. Epub 2011/05/07. doi: 10.1016/j.freeradbiomed.2011.04.026. PubMed PMID: 21545836; PMID: Pmc3997112.

49. Zhao Z, Chen Y, Wang J, Sternberg P, Freeman ML, Grossniklaus HE, Cai J. Age-Related Retinopathy in NRF2-Deficient Mice. *PLoS one*. 2011;6(4):e19456-; PMID: PMC3084871.
50. Felszeghy S, Viiri J, Paterno JJ, Hyttinen JMT, Koskela A, Chen M, Leinonen H, Tanila H, Kivinen N, Koistinen A, Toropainen E, Amadio M, Smedowski A, Reinisalo M, Winiarczyk M, Mackiewicz J, Mutikainen M, Ruotsalainen AK, Kettunen M, Jokivarsi K, Sinha D, Kinnunen K, Petrovski G, Blasiak J, Bjorkoy G, Koskelainen A, Skottman H, Urtti A, Salminen A, Kannan R, Ferrington DA, Xu H, Levonen AL, Tavi P, Kauppinen A, Kaarniranta K. Loss of NRF-2 and PGC-1alpha genes leads to retinal pigment epithelium damage resembling dry age-related macular degeneration. *Redox biology*. 2019;20:1-12. doi: 10.1016/j.redox.2018.09.011. PubMed PMID: 30253279; PMID: PMC6156745.
51. Xiong W, MacColl Garfinkel AE, Li Y, Benowitz LI, Cepko CL. NRF2 promotes neuronal survival in neurodegeneration and acute nerve damage. *The Journal of clinical investigation*. 2015;125(4):1433-45. doi: 10.1172/JCI79735.
52. Wang J, Zhao J, Cui X, Mysona BA, Navneet S, Saul A, Ahuja M, Lambert N, Gazaryan IG, Thomas B, Bollinger KE, Smith SB. The molecular chaperone sigma 1 receptor mediates rescue of retinal cone photoreceptor cells via modulation of NRF2. *Free radical biology & medicine*. 2019;134:604-16. Epub 2019/02/12. doi: 10.1016/j.freeradbiomed.2019.02.001. PubMed PMID: 30743048; PMID: PMC6619428.
53. Ebrahimi KB, Cano M, Rhee J, Datta S, Wang L, Handa JT. Oxidative Stress Induces an Interactive Decline in Wnt and Nrf2 Signaling in Degenerating Retinal Pigment Epithelium. *Antioxid Redox Signal*. 2018;29(4):389-407. Epub 2017/12/01. doi: 10.1089/ars.2017.7084. PubMed PMID: 29186981; PMID: PMC6025703.
54. Sachdeva MM, Cano M, Handa JT. Nrf2 signaling is impaired in the aging RPE given an oxidative insult. *Experimental eye research*. 2014;119:111-4; PMID: PMC3946784.
55. Rabbani N, Shaheen F, Anwar A, Masania J, Thornalley PJ. Assay of methylglyoxal-derived protein and nucleotide AGEs. *BiochemSocTrans*. 2014;42(2):511-7.
56. Pawlak DB, Kushner JA, Ludwig DS. Effects of dietary glycaemic index on adiposity, glucose homeostasis, and plasma lipids in animals. *Lancet*. 2004;364(9436):778-85. PubMed PMID: 15337404.
57. Isken F, Klaus S, Petzke KJ, Loddenkemper C, Pfeiffer AF, Weickert MO. Impairment of fat oxidation under high vs low glycemic index diet occurs prior to the development of an obese phenotype. *Am J Physiol Endocrinol Metab*. 2010;298(2):E297-95. PubMed PMID: 19934403.
58. Pi JB, Leung L, Xue P, Wang WP, Hou YY, Liu DX, Yehuda-Shnaidman E, Lee C, Lau J, Kurtz TW, Chan JY. Deficiency in the Nuclear Factor E2-related Factor-2 Transcription Factor Results in Impaired Adipogenesis and Protects against Diet-induced Obesity. *Journal of Biological Chemistry*. 2010;285(12):9292-300. doi: 10.1074/jbc.M109.093955. PubMed PMID: WOS:000275553700077.
59. Rowan S, Weikel K, Chang ML, Nagel BA, Thinschmidt JS, Carey A, Grant MB, Fliesler SJ, Smith D, Taylor A. Cfh genotype interacts with dietary glycemic index to modulate age-related macular degeneration-like features in mice. *Invest Ophthalmol Vis Sci*. 2014;55(1):492-501. doi: 10.1167/iovs.13-12413. PubMed PMID: 24370827; PMID: PMC3901416.
60. Landowski M, Kelly U, Klingeborn M, Groelle M, Ding JD, Grigsby D, Bowes Rickman C. Human complement factor H Y402H polymorphism causes an age-related macular degeneration phenotype and lipoprotein dysregulation in mice. *Proc Natl Acad Sci U S A*. 2019;116(9):3703-11. doi: 10.1073/pnas.1814014116. PubMed PMID: 30808757.
61. Ufret-Vincenty RL, Aredo B, Liu X, McMahon A, Chen PW, Sun H, Niederkorn JY, Kedzierski W. Transgenic mice expressing variants of complement factor H develop AMD-like retinal findings. *Invest Ophthalmol Vis Sci*. 2010;51(11):5878-87. Epub 2010/06/12. doi: iovs.09-4457 [pii] 10.1167/iovs.09-4457. PubMed PMID: 20538999.
62. Espinosa-Heidmann DG, Sall J, Hernandez EP, Cousins SW. Basal laminar deposit formation in APO B100 transgenic mice: complex interactions between dietary fat, blue light, and vitamin E. *Invest Ophthalmol Vis Sci*. 2004;45(1):260-6. PubMed PMID: 14691182.

63. Zhang M, Chu Y, Mowery J, Konkell B, Galli S, Theos AC, Golestaneh N. Pgc-1alpha repression and high-fat diet induce age-related macular degeneration-like phenotypes in mice. *Dis Model Mech.* 2018;11(9). Epub 2018/06/22. doi: 10.1242/dmm.032698. PubMed PMID: 29925537; PMCID: PMC6176989.
64. Choi W, Moulton EM, Waheed NK, Adhi M, Lee B, Lu CD, de Carlo TE, Jayaraman V, Rosenfeld PJ, Duker JS, Fujimoto JG. Ultrahigh-Speed, Swept-Source Optical Coherence Tomography Angiography in Nonexudative Age-Related Macular Degeneration with Geographic Atrophy. *Ophthalmology.* 2015;122(12):2532-44. Epub 2015/10/21. doi: 10.1016/j.ophtha.2015.08.029. PubMed PMID: 26481819; PMCID: PMC4658257.
65. Sohn EH, Flamme-Wiese MJ, Whitmore SS, Workalemahu G, Marneros AG, Boese EA, Kwon YH, Wang K, Abramoff MD, Tucker BA, Stone EM, Mullins RF. Choriocapillaris Degeneration in Geographic Atrophy. *Am J Pathol.* 2019;189(7):1473-80. Epub 2019/05/06. doi: 10.1016/j.ajpath.2019.04.005. PubMed PMID: 31051169.
66. Terluk MR, Kappahn RJ, Soukup LM, Gong H, Gallardo C, Montezuma SR, Ferrington DA. Investigating mitochondria as a target for treating age-related macular degeneration. *The Journal of neuroscience : the official journal of the Society for Neuroscience.* 2015;35(18):7304-11. Epub 2015/05/08. doi: 10.1523/JNEUROSCI.0190-15.2015. PubMed PMID: 25948278; PMCID: PMC4420790.
67. Kenney MC, Atilano SR, Boyer D, Chwa M, Chak G, Chinichian S, Coskun P, Wallace DC, Nesburn AB, Udar NS. Characterization of retinal and blood mitochondrial DNA from age-related macular degeneration patients. *Invest Ophthalmol Vis Sci.* 2010;51(8):4289-97. Epub 2010/04/02. doi: 10.1167/iovs.09-4778. PubMed PMID: 20357205.
68. Feher J, Kovacs I, Artico M, Cavallotti C, Papale A, Balacco Gabrieli C. Mitochondrial alterations of retinal pigment epithelium in age-related macular degeneration. *Neurobiol Aging.* 2006;27(7):983-93. PubMed PMID: 15979212.
69. Ferrington DA, Ebeling MC, Kappahn RJ, Terluk MR, Fisher CR, Polanco JR, Roehrich H, Leary MM, Geng Z, Dutton JR, Montezuma SR. Altered bioenergetics and enhanced resistance to oxidative stress in human retinal pigment epithelial cells from donors with age-related macular degeneration. *Redox biology.* 2017;13:255-65. Epub 2017/06/11. doi: 10.1016/j.redox.2017.05.015. PubMed PMID: 28600982; PMCID: PMC5466586.
70. Satish S, Philipose H, Rosales MAB, Saint-Geniez M. Pharmaceutical Induction of PGC-1alpha Promotes Retinal Pigment Epithelial Cell Metabolism and Protects against Oxidative Damage. *Oxidative medicine and cellular longevity.* 2018;2018:9248640. Epub 2018/12/14. doi: 10.1155/2018/9248640. PubMed PMID: 30524663; PMCID: PMC6247391.
71. Takahashi A, Takabatake Y, Kimura T, Maejima I, Namba T, Yamamoto T, Matsuda J, Minami S, Kaimori JY, Matsui I, Matsusaka T, Niimura F, Yoshimori T, Isaka Y. Autophagy Inhibits the Accumulation of Advanced Glycation End Products by Promoting Lysosomal Biogenesis and Function in the Kidney Proximal Tubules. *Diabetes.* 2017. Epub 2017/03/02. doi: 10.2337/db16-0397. PubMed PMID: 28246295.
72. Zhang Y, Cross SD, Stanton JB, Marmorstein AD, Le YZ, Marmorstein LY. Early AMD-like defects in the RPE and retinal degeneration in aged mice with RPE-specific deletion of Atg5 or Atg7. *Molecular vision.* 2017;23:228-41. PubMed PMID: 28465655; PMCID: PMC5398883.
73. Rowan S, Bejarano E, Taylor A. Mechanistic targeting of advanced glycation end-products in age-related diseases. *Biochim Biophys Acta Mol Basis Dis.* 2018;1864(12):3631-43. Epub 2018/10/04. doi: 10.1016/j.bbdis.2018.08.036. PubMed PMID: 30279139.
74. Kanow MA, Giarmarco MM, Jankowski CS, Tsantilas K, Engel AL, Du J, Linton JD, Farnsworth CC, Sloat SR, Rountree A, Sweet IR, Lindsay KJ, Parker ED, Brockerhoff SE, Sadilek M, Chao JR, Hurley JB. Biochemical adaptations of the retina and retinal pigment epithelium support a metabolic ecosystem in the vertebrate eye. *Elife.* 2017;6. Epub 2017/09/14. doi: 10.7554/eLife.28899. PubMed PMID: 28901286; PMCID: 5617631.

75. Huang J, Gu S, Chen M, Zhang SJ, Jiang Z, Chen X, Jiang C, Liu G, Radu RA, Sun X, Vollrath D, Du J, Yan B, Zhao C. Abnormal mTORC1 signaling leads to retinal pigment epithelium degeneration. *Theranostics*. 2019;9(4):1170-80. Epub 2019/03/15. doi: 10.7150/thno.26281. PubMed PMID: 30867823; PMCID: PMC6401408.
76. Xu L, Kong L, Wang J, Ash JD. Stimulation of AMPK prevents degeneration of photoreceptors and the retinal pigment epithelium. *Proc Natl Acad Sci U S A*. 2018;115(41):10475-80. Epub 2018/09/27. doi: 10.1073/pnas.1802724115. PubMed PMID: 30249643; PMCID: PMC6187182.
77. Blander JM, Longman RS, Iliev ID, Sonnenberg GF, Artis D. Regulation of inflammation by microbiota interactions with the host. *Nature immunology*. 2017;18(8):851-60. Epub 2017/07/20. doi: 10.1038/ni.3780. PubMed PMID: 28722709.
78. Ardeljan CP, Ardeljan D, Abu-Asab M, Chan CC. Inflammation and Cell Death in Age-Related Macular Degeneration: An Immunopathological and Ultrastructural Model. *J Clin Med*. 2014;3(4):1542-60. Epub 2015/01/13. doi: 10.3390/jcm3041542. PubMed PMID: 25580276; PMCID: PMC4287551.
79. Hollyfield JG, Bonilha VL, Rayborn ME, Yang X, Shadrach KG, Lu L, Ufret RL, Salomon RG, Perez VL. Oxidative damage-induced inflammation initiates age-related macular degeneration. *Nature medicine*. 2008;14(2):194-8. PubMed PMID: 18223656.
80. Doyle SL, Campbell M, Ozaki E, Salomon RG, Mori A, Kenna PF, Farrar GJ, Kiang AS, Humphries MM, Lavelle EC, O'Neill LA, Hollyfield JG, Humphries P. NLRP3 has a protective role in age-related macular degeneration through the induction of IL-18 by drusen components. *Nature medicine*. 2012;18(5):791-8. doi: 10.1038/nm.2717. PubMed PMID: 22484808; PMCID: 3984677.
81. Zinkernagel MS, Zysset-Burri DC, Keller I, Berger LE, Leichtle AB, Largiader CR, Fiedler GM, Wolf S. Association of the Intestinal Microbiome with the Development of Neovascular Age-Related Macular Degeneration. *Sci Rep*. 2017;7:40826. doi: 10.1038/srep40826. PubMed PMID: 28094305; PMCID: PMC5240106.
82. Akiyama K, Warabi E, Okada K, Yanagawa T, Ishii T, Kose K, Tokushige K, Ishige K, Mizokami Y, Yamagata K, Onizawa K, Ariizumi SI, Yamamoto M, Shoda J. Deletion of both p62 and Nrf2 spontaneously results in the development of nonalcoholic steatohepatitis. *Exp Anim*. 2018;67(2):201-18. Epub 2017/12/26. doi: 10.1538/expanim.17-0112. PubMed PMID: 29276215; PMCID: PMC5955752.
83. Thaiss CA, Levy M, Grosheva I, Zheng D, Soffer E, Blacher E, Braverman S, Tengeler AC, Barak O, Elazar M, Ben-Zeev R, Lehavi-Regev D, Katz MN, Pevsner-Fischer M, Gertler A, Halpern Z, Harmelin A, Amar S, Serradas P, Grosfeld A, Shapiro H, Geiger B, Elinav E. Hyperglycemia drives intestinal barrier dysfunction and risk for enteric infection. *Science*. 2018;359(6382):1376-83. Epub 2018/03/10. doi: 10.1126/science.aar3318. PubMed PMID: 29519916.
84. Singh R, Chandrashekhara S, Bodduluri SR, Baby BV, Hegde B, Kotla NG, Hiwale AA, Saiyed T, Patel P, Vijay-Kumar M, Langille MGI, Douglas GM, Cheng X, Rouchka EC, Waigel SJ, Dryden GW, Alatassi H, Zhang HG, Haribabu B, Vemula PK, Jala VR. Enhancement of the gut barrier integrity by a microbial metabolite through the Nrf2 pathway. *Nat Commun*. 2019;10(1):89. Epub 2019/01/11. doi: 10.1038/s41467-018-07859-7. PubMed PMID: 30626868; PMCID: PMC6327034.
85. He C, Huang L, Lei P, Liu X, Li B, Shan Y. Sulforaphane Normalizes Intestinal Flora and Enhances Gut Barrier in Mice with BBN-Induced Bladder Cancer. *Mol Nutr Food Res*. 2018;62(24):e1800427. Epub 2018/10/12. doi: 10.1002/mnfr.201800427. PubMed PMID: 30302904.
86. Axelsson AS, Tubbs E, Mecham B, Chacko S, Nenonen HA, Tang Y, Fahey JW, Derry JM, Wollheim CB, Wierup N, Haymond MW, Friend SH, Mulder H, Rosengren AH. Sulforaphane reduces hepatic glucose production and improves glucose control in patients with type 2 diabetes. *Science translational medicine*. 2017;9(394). Epub 2017/06/16. doi: 10.1126/scitranslmed.aah4477. PubMed PMID: 28615356.
87. Scribner KB, Pawlak DB, Ludwig DS. Hepatic steatosis and increased adiposity in mice consuming rapidly vs. slowly absorbed carbohydrate. *Obesity (Silver Spring)*. 2007;15(9):2190-9. PubMed PMID: 17890486.

